Area Law Violations in Entanglement Measures for Disordered and Inhomogeneous Quantum Spin Chains

AC38091

September 2022

Abstract

In this report, we investigate the scaling of different measures of entanglement in disordered and inhomogeneous XXY spin-$\frac{1}{2}$ chains. We first discuss how entanglement can be measured with the entanglement entropy and logarithmic negativity, before discussing the entanglement area law and known violations to the area law. We focus on two previously studied systems that violate the area law: disordered spin chains and inhomogeneous disordered spin chains whose couplings decay exponentially quickly from the centre of the chain. Our review includes analytical results from the Strong Disorder Renormalisation Group (SDRG) method that show that entanglement in the disordered spin chain increases with the logarithm of the subsystem length, and that entanglement in the inhomogeneous disordered spin chain increases as a square root of the subsystem length. We also verify a number of results on entanglement area law violations by implementing the SDRG method numerically. Firstly, we verify results on the entanglement entropy and logarithmic negativity for disordered models and on the entanglement entropy for the inhomogeneous disordered models. Then, we derive a simple analytic expectation for the logarithmic negativity of the inhomogeneous disordered chain via the SDRG method, and verify that numerically. Lastly, we investigate inhomogeneous disordered systems whose couplings decay as a power-law from the centre of the chain. Whilst we are not able to derive any analytic results for these systems, we show via the numerical SDRG method that the power-law scaling does not seem to survive, and the results are closer to those of the disordered homogeneous system.

Contents

1 Introduction **3**

2 Measures of Entanglement **4**
2.1 Entanglement as an Information Phenomenon 4
2.2 Entanglement Entropy and Logarithmic Negativity 4
2.3 Entanglement Area Law Violations in Quantum Systems 5

3 The Random Inhomogeneous Chain and the SDRG method **7**
3.1 The Random Inhomogeneous Chain 7
3.2 SDRG Literature Review 7
3.3 SDRG Procedure 8
3.4 Algorithmic Implementation and Complexity 10

4 Disordered Chain: Existing Results **13**
4.1 Entanglement Entropy: Analytic Results and Numerical SDRG 13
4.2 Logarithmic Negativity: Analytic Results and Numerical SDRG 14

5 Randbow Chain: Existing Results **17**
5.1 Entanglement Entropy: Analytic Results 17
5.2 Entanglement Entropy: Numerical SDRG 18
5.3 Randbow Chain Exact Solution 19

6 Logarithmic Negativity for the Randbow Chain **23**
6.1 Analytical Expectation 23
6.2 Numerical SDRG 23

7 Power-Law Spin Chains **26**
7.1 Analytic Results 26
7.2 Entanglement Entropy: SDRG and exact results 26
7.3 Logarithmic Negativity Scaling: SDRG 27
7.4 Possible explanations 27

8 Conclusion **32**

A Quantum Mechanics and the Jordan-Wigner Transformation **33**
A.1 Commutators 33
A.2 Spin 33
A.3 The Jordan-Wigner Transformation 34
A.4 Using the JW Transformation in the Exact Solution 34

1 Introduction

Entanglement is the phenomenon of correlation between distantly separated objects. In a quantum system, a number of objects can be 'entangled' such that operations on one particle instantaneously affects the other entangled particles, even when these particles have no apparent connection to the first.

Researchers are especially interested in how the entanglement of a subsystem changes with the subsystem size: does entanglement increase with the area of a subsystem, with its volume, or something else? The claim that in some systems, entanglement scales with area, is known as the *entanglement area law*. Systems whose entanglement does not scale with the area are said to exhibit area law violations, and understanding area law violations has become an important avenue of research [1].

The area law is known to hold for certain measures of entanglement in specific conditions. For example, for local, gapped, spatially invariant one dimensional quantum systems in their groundstate, entanglement entropy (one measure of entanglement that will be defined later) scales with an area law [2]. However, attempts to generalise this to weaker conditions have shown that area law violations may occur [3]. Thus the research question becomes: 'Which of the assumptions in [2] when relaxed are necessary or sufficient conditions to lead to an area law violation, and what scaling do we observe when these violations occur?'.

This report extends the work of two papers ([4] and [5]) that have answered this question in the context of quantum spin chains. The authors studied the entanglement scaling of spin chains with varying degrees of disorder and inhomogeneity, both of which violate the spatially invariant condition in [2]. In [4], the authors reproduced results from [3] that in disordered quantum spin chains, the entanglement entropy scales with the logarithm of the subsystem size, and then showed that the logarithmic negativity (another measure of entanglement that will be defined later) also scales logarithmically. In [6] the authors show that when inter-spin couplings decay exponentially from the centre of the chain, a volume law for the entanglement entropy can occur. In [5], the authors extend that work by showing that an intermediate phase exists where the inhomogeneity is less strong and the entanglement entropy scales as a power-law.

Both [4] and [5] make use of the Strong Disorder Renormalisation Group (SDRG). Whilst disorder and inhomogeneity introduce a new richness of modelling possibilities, they also produce complex systems that are difficult to solve. This has prompted a wave of techniques based on renormalisation group (RG) theory [7], which has been extended to SDRG for disordered systems [8]. The SDRG approach maps a disordered problem to a simpler one by progressively integrating out the high energy degrees of freedom. This provides us with an approximation of the system's groundstate that is easier to calculate than the true groundstate. The SDRG method is useful both for analytic results and as a numerical method. Exact results for the outcome of the SDRG procedure and for analyses on the resulting SDRG groundstate are available and are used in the two papers, which also make use of an exact solution that is available when the system is non-interacting. This report extends their work by calculating the logarithmic negativity of the inhomogeneous system introduced in [5], and by investigating a new kind of system with a weaker degree of inhomogeneity where couplings decay as a power-law from the chain centre.

The structure of this report is as follows. In section 2, we review measures of entanglement and area law violations. In section 3, we state spin chain models to be investigated and the SDRG procedure. In sections 4 and 5.1 we will verify existing results, and in sections 6 and 7 we will demonstrate the new results on entanglement negativity for old systems and for the new slowly decaying systems. Lastly, in section 8 we will evaluate the new results and discuss areas for further research. In the appendix, we review some relevant quantum physics and the Jordan-Wigner transformation. We assume that the reader is familiar with basic quantum physics and especially bra-ket notation.

2 Measures of Entanglement

2.1 Entanglement as an Information Phenomenon

Calculating the amount of entanglement in a system is a non-trivial problem. A system is defined as being entangled entangled if and only if (iff) it is not *separable* [9]. To define separability, we first note that any state $|\psi\rangle$ in a Hilbert space $\mathcal{H}$ can be expressed as a density matrix ρ:

$$\rho = |\psi\rangle \langle\psi| \tag{2.1}$$

Separability implies that, given a set of classical probabilities $\{p_i\}$, and a set of density matrices for two subsystems A and B, any density matrix ρ for the space $\mathcal{H} = \mathcal{H}_A \otimes \mathcal{H}_B$ can be written as:

$$\rho = \sum_i p_i \rho_A^i \otimes \rho_B^i \tag{2.2}$$

Given a such a density matrix ρ, research has often turned to an axiomatic approach for measures on entanglement. This involves stating what conditions a measure of entanglement must satisfy to be considered useful. There is a significant debate around what these axioms should be: see [10] and [11] for examples. We will follow [9] and use the following three conditions for a measure of entanglement E:

1. *Monotonicity*: $E(\rho) \geq \sum_i E(\Theta(\rho))$ for some LOCC operation Θ
2. *Convexity*: $\sum_i p_i E(\rho_i) \geq E\left(\sum_i p_i \rho_i\right)$
3. *Additivity under the tensor product*: $E\left(\otimes_i \rho_i\right) = \sum_i E\left(\rho_i\right)$

Monotonicity implies that any classical interference with the state (represented by the operation Θ) can only lower its entropy. This is one requirement for keeping measures of entanglement focused strictly on the quantum correlations. The convexity condition implies that a classical mixing of states cannot produce entanglement, and the additivity requirement is exceptionally useful as it permits the simple calculation of states formed of the tensor product of many substates. We will come across such states frequently later in the report.

2.2 Entanglement Entropy and Logarithmic Negativity

Having established a framework for understanding different measures of entanglement, we will now define the key measures used in this report. We start by defining the generalised Rényi entropies [12]:

$$S_n\left(\rho_A\right) = \frac{1}{1-n} \log \operatorname{Tr} \rho_A^n \tag{2.3}$$

where ρ_A is the reduced density matrix over the subsystem A, found by taking the partial trace over the B subsystem with bases $|j_B\rangle$:

$$\rho_A = \operatorname{Tr}_B[\rho] = \sum_j \langle j|_B \rho |j\rangle_B \,^1 \tag{2.4}$$

Note that all Rényi entropies are symmetric with respect to the subsystem, i.e. $S_n\left(\rho_A\right) = S_n\left(\rho_B\right)$ [9]. Unfortunately, Rényi entropies do not satisfy the useful subadditivity condition:

$$S\left(\rho_{A\cup B}\right) \leq S\left(\rho_A\right) + S\left(\rho_B\right) \tag{2.5}$$

for bipartite systems $A \cup B$. Fortunately, taking the limit $n \to 1$ we recover the von Neumann entanglement entropy, which is subadditive [13]:

[1] Note that in this notation, there is an implied identity operator I in the operation $\langle j|_B \rho$, i.e. $(I \otimes \langle j|_B)\rho$, and similarly for the ket, to ensure that the dimensions of the bra and the density matrix match.

$$S(\rho_A) = -\operatorname{Tr}(\rho_A \log \rho_A) \tag{2.6}$$

The von Neumann entanglement entropy, which we will refer to throughout as the entanglement entropy, satisfies all three of the axioms for measures of entanglement.

Unfortunately, the entanglement entropy is only a good measure of entanglement if the system is in a pure state and if it is bipartite - otherwise classical correlations will interfere [9]. The only other calculable forms of entanglement are those related to the *negativity*. Before defining negativity, we define the partial transpose $\rho_A^{T_2}$ of a reduced density matrix ρ_A:

$$\langle \varphi_A \varphi_B | \rho_A^{T_2} | \varphi'_A \varphi'_B \rangle \equiv \langle \varphi_A \varphi'_B | \rho_A | \varphi'_A \varphi_B \rangle \tag{2.7}$$

where $\{\varphi_X\}$ is a basis for subsystem X [4]. We also define the trace distance $||A||$ of an operator A:

$$||A|| = \operatorname{Tr} \sqrt{AA^\dagger} \tag{2.8}$$

Assuming A is Hermitian, the trace distance of A is the sum of the absolute value of the eigenvalues of A [9]. We can now define the negativity:

$$\mathcal{N}(\rho_A) = \frac{||\rho_A^{T_2}|| - 1}{2} \tag{2.9}$$

Whilst this is monotone and convex, it is not additive under the tensor product. However, we can take the logarithmic form, which is additive under the tensor product, giving us the logarithmic negativity $\mathcal{E}$:

$$\mathcal{E}(\rho_A) = \ln ||\rho_A^{T_2}|| \tag{2.10}$$

Whilst the logarithmic negativity is not convex, it is monotone and additive and forms a good measure of entanglement [11].

2.3 Entanglement Area Law Violations in Quantum Systems

Having defined entanglement and two entanglement measures, we will briefly survey the wide literature of area law violations in quantum systems. We will recap that which was mentioned briefly in the introduction, that in 2004 Hastings published a proof of the area law for local, gapped, translationally invariant systems in one dimension in their groundstate [2], i.e. Hamiltonians of the form:

$$H = \sum_{i=1}^{N} H_{i,i+1} \tag{2.11}$$

where $H_{i,i+1}$ is a function only of the sites i and $i+1$. Note that this applies strictly to systems in their groundstate ([14], [1]).

This area law sets a baseline for the physics of such systems. The fact that systems do in fact display area law violations of their quantum entropy (e.g. [15]) has prompted aresearch to identify and explain these phenomena. For example, Calabrese and Cardy [16] give a thorough treatment through $(1+1)d$ conformal field theory (CFT) of the entanglement entropy, and show that the entropy S_A of a subsystem A of length l at zero temperature in an infinitely long, 1D system without boundaries is:

$$S_A \sim (c/3) \log (l/a) \tag{2.12}$$

where c is the central charge and a is the lattice spacing. This is known as a logarithmic correction to the area law. Similarly, Calabrese et al. compute the scaling of the logarithmic negativity in the CFT framework and show that it scales logarithmically in l [17].

Before we introduce the model investigated in this report in detail, it is useful to point out that the behaviour of most such models depends on the inter-spin couplings $\{J\}$. This will let us summarise a number of results for spins chains that lay the groundwork for this report. In 1980, Dasgupta & Ma

demonstrated an SDRG rule for disordered spin chains which gradually lowers the energy level of the couplings $\{J\}$, and showed that the result of the said procedure was a random singlet phase (RSP) [8]. An RSP is a collection of singlets (pair of spins) where the spins in each singlet are entangled with each other and no other spins. In 2004, Refael & Moore showed that the mean entanglement entropy of a subsystem l in a disordered spin chain also scales as $\ln l$ [3]. Their result was derived analytically within the SDRG approach, and they showed in particular that under the steps of the SDRG process the distribution of the couplings $\{J\}$ approaches a fixed point. Then, in 2010, Vitagliano et al. presented the 'rainbow chain' by introducing an inhomogeneous factor, alongside the disordered factor, for the initial couplings that decayed exponentially quickly from the centre of the chain [6]. When this inhomogeneous component is very strong, bonds in the centre of the chain are guaranteed to be eliminated first, and the RSP looks like a rainbow: every singlet link is symmetric with respect to the centre of the chain. For the rainbow phase it is easy to show that the entanglement entropy scales as a volume law.

This brings us to the two central papers for this report. In 2016, Ruggiero et al. verified the logarithmic scaling of the entanglement entropy in disordered chains numerically with SDDG, as well as showing that the logarithmic negativity also scales logarithmically. Again, this was shown analytically with SDRG and then verified with a numerical implementation of SDRG. Lastly, in 2019, Alba et al. showed that the rainbow chain introduced in [6] could be modified so as to make the inhomogeneous factor in the couplings weaker. This introduced the 'randbow' phase, where some singlets are rainbows, symmetric with respect to the centre of the chain, and others are 'bubbles', with adjacent spins entangled. The entanglement entropy of the randbow system is a power-law.

As well as verifying these existing results, our report will be exploring the logarithmic negativity of the randbow chain, and the entanglement entropy and the logarithmic negativity of a system between the disordered chain and the randbow chain where couplings decay as a power-law from the centre of the chain. In the following section we will outline the principle model that we study as well, as the SDRG procedure. This will also allow us to explain how entropy measures are calculated in the simulations we conduct.

3 The Random Inhomogeneous Chain and the SDRG method

3.1 The Random Inhomogeneous Chain

The random inhomogeneous spin-$\frac{1}{2}$ XXZ chain with L spins and open boundary conditions (OBC) has the Hamiltonian:

$$H = \sum_{i=1}^{L-1} J_i \left(S_i^x S_{i+1}^x + S_i^y S_{i+1}^y + \Delta S_i^z S_{i+1}^z \right) \tag{3.1}$$

where $S_i^x = \frac{\hbar}{2}\sigma_x$ and σ_i^x is a Pauli matrix acting on site i, J_i is a coupling connecting site i to $i+1$, and Δ is an anisotropy parameter. In all cases we restrict ourselves to even numbers of spins, i.e. even L. For periodic boundary conditions (PBC) an additional term for $i = L$ is needed. With $\Delta = 1$ we have the XXX chain and with $\Delta = 0$ we have the XX chain. With the XX chain the model is exactly solvable [4].

Here we will give the most general form of the couplings:

$$J_i = K_i \times F(i) \tag{3.2}$$

where F is function that depends deterministically on i, and K_i is a random variable with the following distribution:

$$P_\delta(J) \equiv \delta^{-1} J^{-1+1/\delta} \tag{3.3}$$

Clearly as $\delta \to 0$ the distribution peaks at 1 and taking $F(i) = 1$ we recover the clean spin chain. For $\delta \to 1$ we approach a uniform distribution on $[0, 1]$. As $\delta \to \infty$ we approach the infinite randomness fixed point (IRFP), which describes the asymptotic state of the distribution of $\{J_i\}$ under successive SDRG steps [7].

In this report, we will frequently refer to a subsystem centred in a one dimensional chain. To make this clear, we present in figures 3.1 and 3.2 the two key subsystem scenarios. In figure 3.1, we show a single subsystem A in the centre of the chain. Notice that the the subsystem A starts with the right hand spin of the two spins connected by coupling J_0. Unless otherwise stated, subsystems will always start from the centre of the chain in this way. In figure 3.2, we show two disjoint subsystems A_1 and A_2, with a region r separating them. We restrict ourselves to even r in simulations. In the case of periodic boundary conditions, the bond extending from site L will connect around into site 1. In open boundary conditions, spin L will have a bond $J_L = 0$ which eliminates that interaction from the system.

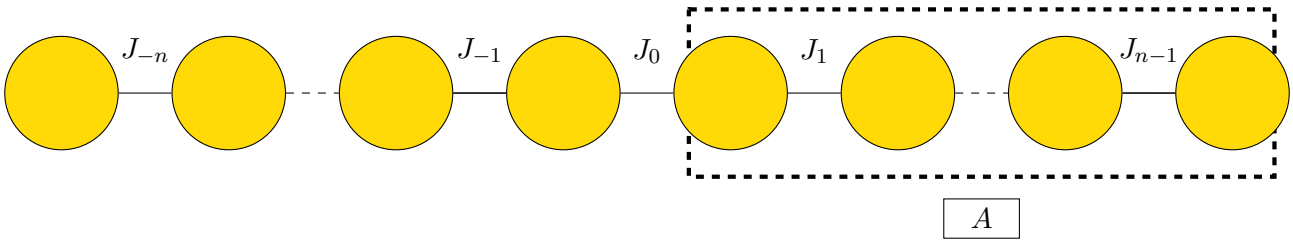

Figure 3.1: A spin chain with the central bond labelled J_0. The subsystem A is highlighted with the dashed line.

3.2 SDRG Literature Review

Whilst in non-interacting cases, spin chain models are often exactly solvable, this is not the case in general. The RG approach to approximating complex systems (quantum and classical) came out of work with (Michael) Fisher and Wilson in the 1960s [18]. RG involves successively integrating out the high energy degrees of freedom in a model to approach an approximation of the system's groundstate. Each RG step f maps the problem $H(J)$ to a new problem $f(H(J)) = H(J')$, with fewer degrees of freedom. Iterating this process will lead to a point where the transformation $f(H(J^\star)) = H(J^\star)$ is a

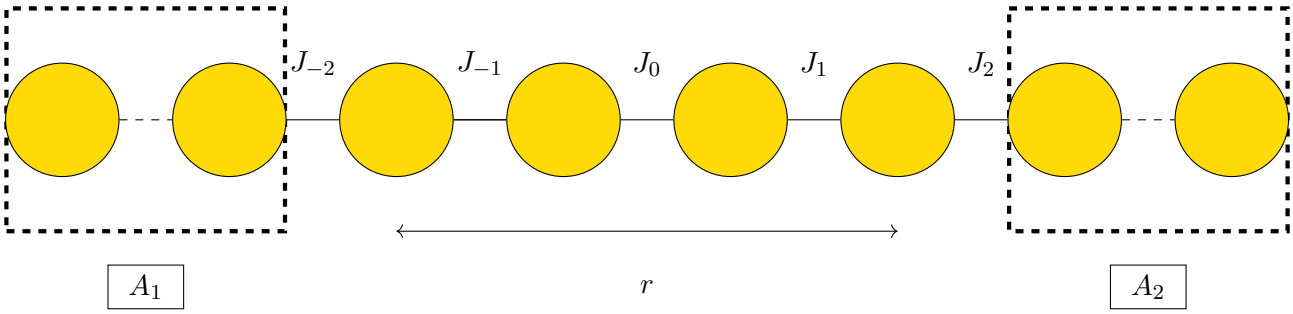

Figure 3.2: A spin chain with a pair of disjoint subsystems, separated by a distance r. The subsystems A_1 and A_2 are highlighted with the dashed line.

fixed point. This is especially useful in complex models such as many bodied systems: the fixed point is simpler to find and analyse than the true solution, whilst capturing the relevant physical properties of the original model.

In this paper we will focus on disordered models, for which we use the strong disorder renormalisation group (SDRG). For a very thorough review, see [19] and [20]. The difference between SDRG and other forms of RG for spins chains is that SDRG renormalises space 'in an inhomogeneous way in order to adapt better to the local disorder fluctuations' [19]. For disordered spin chains, each SDRG step changes the distribution of the remaining couplings $\{J\}$, as well as eliminating two spins, and the 'flow' of the successive distributions $P(J) \to P(J')$ characterises the SDRG process. The fixed point of this distribution as it changes under SDRG steps is called the infinite randomness fixed point (IRFP). The key contribution was from Dasgupta, Ma, and Hu ([21], [8]) who defined the elimination rule that was generalised by (Daniel) Fisher [7]. Since then the SDRG procedure has been used to investigate a great variety of challenging disordered problems ([22], [23], [24], [3]).

3.3 SDRG Procedure

We will summarise the SDRG procedure for the inhomogeneous spin chain following [4]. To begin each SDRG step, we identify the strongest coupling J_M and consider the energy of this interaction H_0:

$$H_0 = J_M \vec{S}_l \cdot \vec{S}_r \tag{3.4}$$

The groundstate of this microsystem is:

$$|s\rangle \equiv 2^{-1/2} \left(|\uparrow_l \downarrow_r\rangle - |\downarrow_l \uparrow_r\rangle \right) \tag{3.5}$$

where $\{\uparrow, \downarrow\}$ are up and down basis vectors for the single spin Hilbert space. The two spin state vectors are generated by the tensor product, e.g. $|\uparrow_l \downarrow_r\rangle = \uparrow_l \otimes \downarrow_r$. Treating equation 3.5 as a perturbation[2], we can calculate a new effective coupling between the spins $l-1$ and $r+1$:

$$J' = \frac{J_l J_r}{(1+\Delta) J_M} \tag{3.6}$$

We remove the spins connected by J_M and insert the coupling J' between J_l and J_r. The removed spins are recorded in a list that will be the RSP result of the SDRG procedure. Repeating this process identifies a flow of couplings between steps:

$$(\cdots, J_l, J_M, J_r, \cdots)_L \to \left(\cdots, \frac{J_l J_r}{(1+\Delta) J_M}, \cdots \right)_{L-2} \tag{3.7}$$

Importantly, given that $J_M > J_{(l/r)}$, the new coupling J' is smaller than either, so the energy scale of the system is lowered. The process is then repeated until there are only two spins remaining, which

[2]Details of the perturbation calculations can be found in [4] as well.

become the final singlet. The RSP is a vector of $L \div 2$ singlets - calling this $\{|s\rangle_i\}$, the groundstate as approximated by the SDRG procedure is:

$$|GS\rangle = \bigotimes_{i=1}^{L\div 2} |s\rangle_i \tag{3.8}$$

This approximation of the true groundstate via the SDRG procedure is the random singlet phase (RSP) as introduced in the introduction (section 2.3). This is the first of two 'outputs' of SDRG, the second being the flow of couplings across subsequent SDRG steps. It is this flow of couplings the characterises the progression from the initial distribution $P(J)$ to the the IRFP.

The distribution of couplings can be given in terms of the SDRG step m, following [7]. We introduce the logarithmic variables:

$$\beta_i^{(m)} \equiv \ln \frac{J_M^{(m)}}{J_i^{(m)}}, \quad \Gamma^{(m)} \equiv \ln \frac{J_M^{(0)}}{J_M^{(m)}} \tag{3.9}$$

where $J_M^{(m)}$ is the strongest coupling at the SDRG step m. The flow equation to be solved is given by [7] as:

$$\frac{dP}{d\Gamma} = \frac{\partial P(\beta)}{\partial \beta} P(0) \times \int_0^\infty d\beta_1 \int_0^\infty d\beta_2 \delta\left(\beta - \beta_1 - \beta_2\right) P\left(\beta_1\right) P\left(\beta_2\right) \tag{3.10}$$

which is solved with the ansatz:

$$P^*(\beta) = \frac{1}{\Gamma} \exp\left(-\frac{\beta}{\Gamma}\right) \tag{3.11}$$

Equation 3.10 is the IRFP and is an attractor for any initial distribution of the couplings.

As an initial test of the numerical SDRG procedure we have implemented, we track the flow of the logarithmic couplings in figure 3.3. This is a close reproduction of a similar figure in [4] and shows that the SDRG process is indeed working correctly.

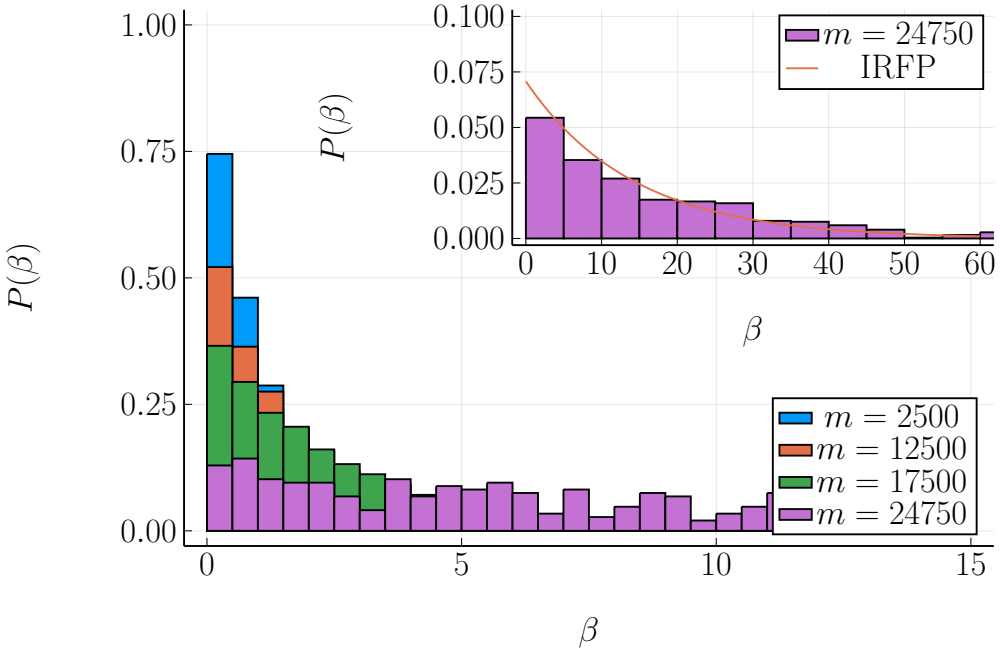

Figure 3.3: SDRG flow for $L = 50,000$ spins in the disordered XXX chain with $\delta = 1$. The main plot shows the β distribution of the remaining bonds at the m^{th} step of the SDRG process. Notice that over SDRG steps, the distribution approaches the IRFP. The inset plot shows subset of the β distribution late into the SDRG process with the IRFP line overlayed. The data is an excellent fit to the analytic prediction.

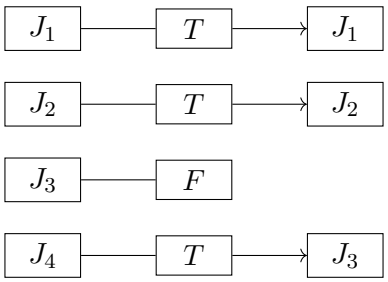

Figure 3.4: Diagram of the data masking procedure used to iteratively eliminate the bonds from the data vector. The approach is size stable so minimises the need for allocations during the procedure.

3.4 Algorithmic Implementation and Complexity

We will briefly detail the SDRG algorithm we have implemented for this report. In studying disordered systems, we frequently need to take averages over disorder, i.e. many different realisations of the system in question. In many cases the number of trials must be very large for the required observables to converge - see [25] and [4] for examples of these issues. Thus an efficient and reliable algorithm is essential.

The key feature of our SDRG implementation is that it is almost memory static - that is, little or no extra memory is allocated in the computer every time a new disorder realisation is run. Rather, the existing memory used to hold data (e.g. bond strengths) is updated at the start of each realisation, and during the elimination process a 'mask' vector is maintained that tracks which bonds are active and should be used in calculation. The one-off allocation of this mask vector is computationally very cheap compared to continually reallocating previous memory. An illustration of this approach can be seen in figure 3.4 and a psuedo-code version of our implementation can be seen in table 1.

Algorithm 1: SDRG algorithm

Data: $\{J\}, L, \{(s_1, s_2)\}$
Result: $\{(s_1, s_2)\}$
$m \leftarrow 1$;
$active \leftarrow \{T\}^L$;
$n\_active = sum(active)$; `// will be used to track the number of active spins`
while $n\_active > 2$ **do**
  $J_M \leftarrow max\{(J_i\}$;
  $J_l \leftarrow J_{M-1}$;
  $J_r \leftarrow J_{M+1}$;
  $J' \leftarrow \frac{J_l J_l}{(1+\Delta)J_M}$;
  $J_l = J'$;
  $active_M \leftarrow F$;
  $active_{M+1} \leftarrow F$;
  $\{(s_1, s_2)\}_m \leftarrow \{(M, M+1)\}$;
  $m \mathrel{+}= 1$;
  $n\_active = sum(active)$;
end
$\{(s_1, s_2)\}_{L \div 2} \leftarrow \{(J_1, J_2)\}$;
return $\{(s_1, s_2)\}$;

To give an estimate of the speed of this procedure, we benchmark the code for varying levels of machine precision and vary system lengths L. The results can be seen in figure 3.5. The elimination procedure for a system of $L = 1000$ spins is on the order of four microseconds. This implies that upwards of $200,000$ SDRG eliminations can be calculated in one second.

In practice, the analysis calculations slow down the 'rate of realisations' considerably. To demonstrate this, we calculate the time taken to calculate the entanglement entropy S over a system of

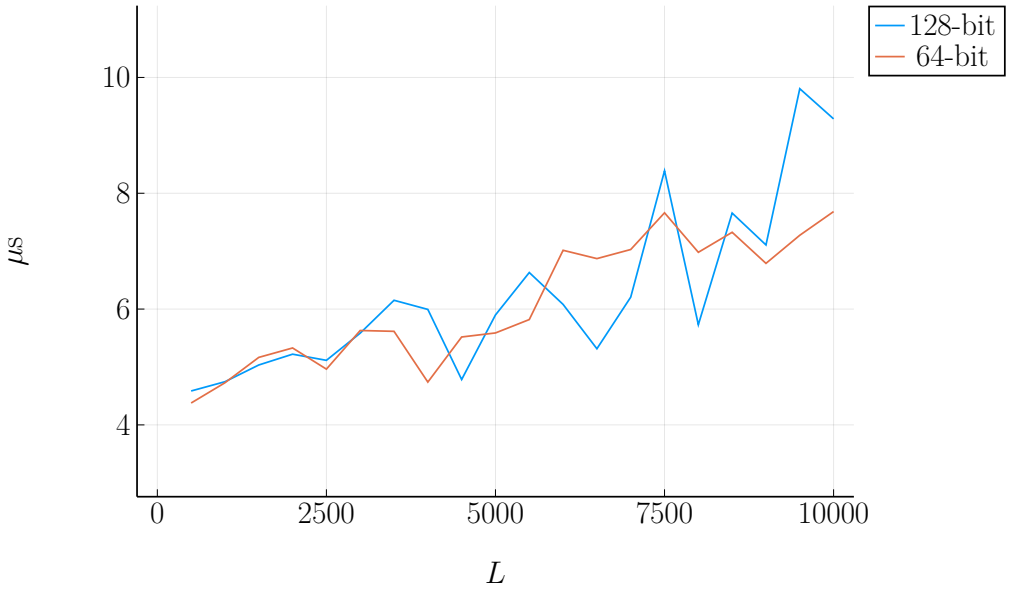

Figure 3.5: Benchmark results for our SDRG procedure. On the horizontal axis we measure the system length L, and on the vertical we report the median execution time for the complete SDRG procedure in microseconds. The execution time increases linearly in the system length for systems L in the order of thousands, and there is only a small performance penalty for using quadruple precision floating point numbers (i.e. 128 bits).

size L for $l \in [1, L \div 2]$ across N disorder realisations, at 64 and 128-bit accuracy within the SDRG procedure. Our results are shown in figure 3.6. In general we observe roughly linear scaling in both L and N. Calculating the entanglement entropy of a system of length 2000 across 2000 disorder realisations takes around 12 seconds, regardless of the floating point definition. This is acceptable for the immediate verification of results and could probably be improved upon considerably with refinements to the analysis code, and the refactoring of the code to work on distributed systems (e.g. industrial level high performance computers (HPCs)).

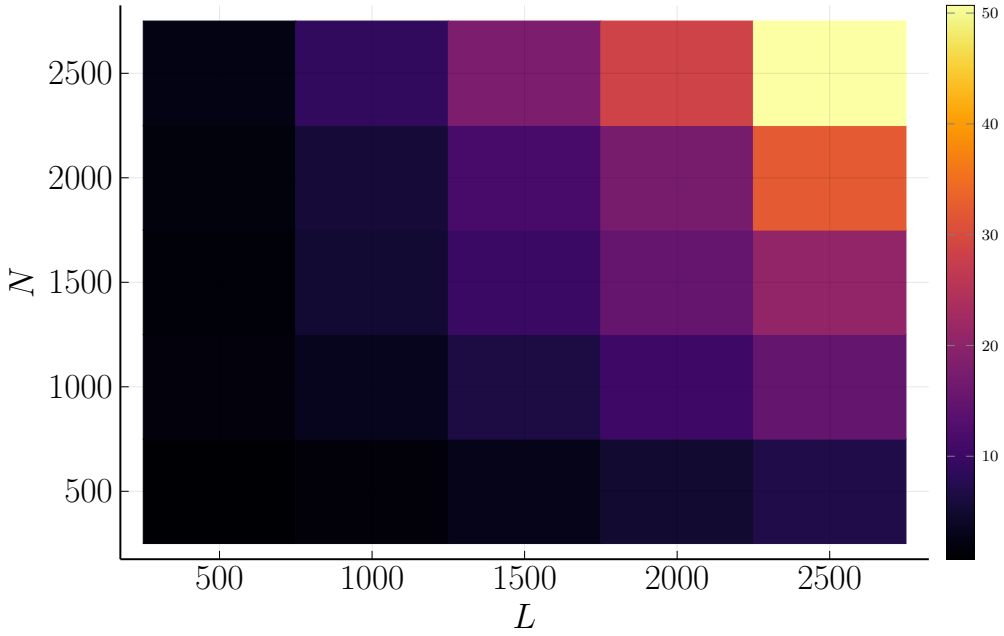

(a) Heatmap of the execution time in seconds to calculate the entanglement entropy S of system of length L for $l \in [1, L \div 2]$ across N disorder realisations at 64-bit accuracy. The colour represents the execution time in seconds.

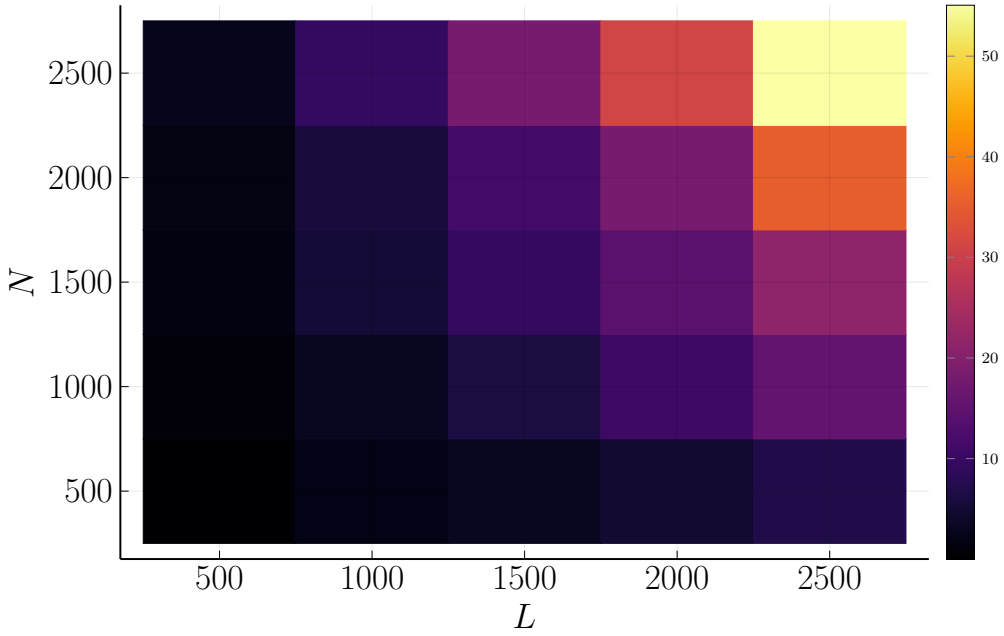

(b) Heatmap of the execution time in seconds to calculate the entanglement entropy S of system of length L for $l \in [1, L \div 2]$ across N disorder realisations at 128-bit accuracy. The colour represents the execution time in seconds.

Figure 3.6: Heatmap of the execution time in seconds to calculate the entanglement entropy S of system of length L for $l \in [1, L \div 2]$ across N disorder realisations at 64- and 128-bit accuracy. The colour represents the execution time in seconds. Notice that the two heatmaps are almost identical to the human eye, which suggests that the floating point size is not a bottleneck for this implementation. Figure 3.6a: timings for 64-bit accuracy in the SDRG procedure. Figure 3.6b: timings for 128-bit accuracy in the SDRG procedure.

4 Disordered Chain: Existing Results

In this section we will reproduce the results of [4] for the disordered spin chain and in the process verify that our SDRG algorithm and related code works as expected.

4.1 Entanglement Entropy: Analytic Results and Numerical SDRG

As per [4], we measure the entanglement entropy of the disordered chain with and without periodic boundary conditions. We start be reviewing the analytic expectations for the disordered spin chain with the SDRG method.

We observe that, given the RSP state in equation 3.8, to calculate the entanglement entropy we only need to know the number of singlets in A that connect to the remainder of the chain $B = A'$. In the basis $|\uparrow\rangle = \begin{bmatrix}1\\0\end{bmatrix}$ and $|\downarrow\rangle = \begin{bmatrix}0\\1\end{bmatrix}$ we can make the singlet state $|s\rangle$ (see equation 3.5) explicit. The two spin vectors become:

$$|\uparrow\downarrow\rangle = \begin{bmatrix}0\\1\\0\\0\end{bmatrix}, |\downarrow\uparrow\rangle = \begin{bmatrix}0\\0\\1\\0\end{bmatrix} \tag{4.1}$$

Recalling the singlet state vector (equation 3.5), the singlet density matrix is then:

$$\rho_{2S} = |s\rangle\langle s| = \frac{1}{2}\begin{pmatrix}0&0&0&0\\0&1&-1&0\\0&-1&1&0\\0&0&0&0\end{pmatrix} \tag{4.2}$$

Taking the partial trace over the second spin, we have:

$$\rho_S = \frac{1}{2}\begin{pmatrix}1&0\\0&1\end{pmatrix} \tag{4.3}$$

To calculate the entanglement entropy, we note that ρ_S is Hermitian and use the spectral theorem on equation 2.6 to get:

$$S = -\sum_i \lambda_i \ln \lambda_i = \ln 2 \tag{4.4}$$

where $\{\lambda_i\}$ are the eigenvalues of ρ_S. At this point, the RSP structure of the grounstate becomes very useful. Following [3] we can say that the entanglement entropy is just 'the number of singlets that connect sites inside to sites outside the segment', multiplied by the entropy of each such segment, $\ln 2$. This is a very simple expression of the entropy for a complex many-body system. We follow [4] and let the number of singlets connecting subsystem X to Y be $n_{X:Y}$, so that the entropy of subsystem A is given by:

$$S_A = \ln 2 \times n_{A:B} \tag{4.5}$$

This is consistent up to a constant with the SDRG result as reported in [4] and [26]:

$$S_A = \frac{\ln 2}{3}\ln \ell + K \tag{4.6}$$

which implies that, taking averages over disorder, $\langle n_{A:B}\rangle = \frac{\ln 2}{3}$.

To verify this numerically, we run the SDRG procedure on the XXX chain: for each simulation, we draw L random couplings from the uniform distribution over $[0, 1]$ and run the SDRG algorithm. This returns a vector of $L \div 2$ singlets. On this vector of singlet pairs we calculate the entanglement entropy for every realisation of the RSP for all window sizes l, and maintain a running mean of the result.

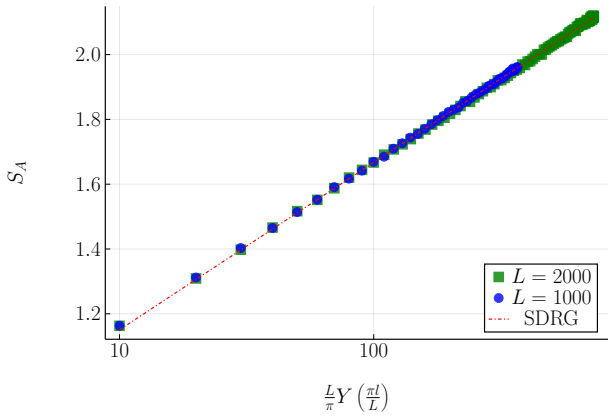

(a) Entanglement entropy of the XXX chain, adjusted l, PBC

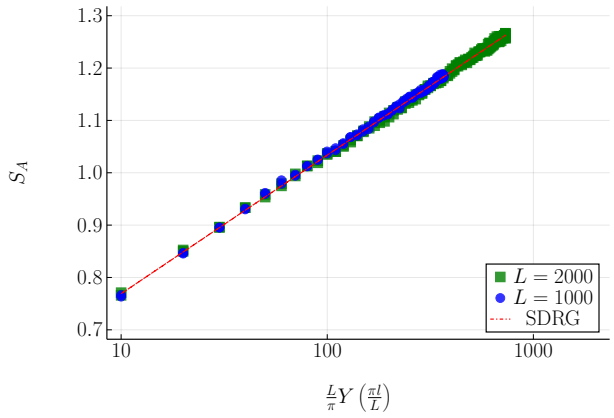

(b) Entanglement entropy of the XXX chain, adjusted l, OBC

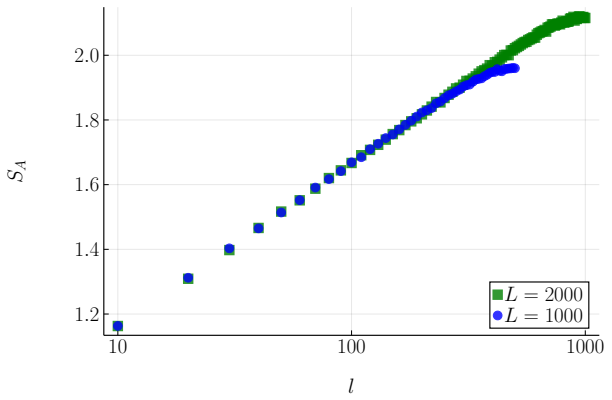

(c) Entanglement entropy of the XXX chain, no l adjustment, PBC

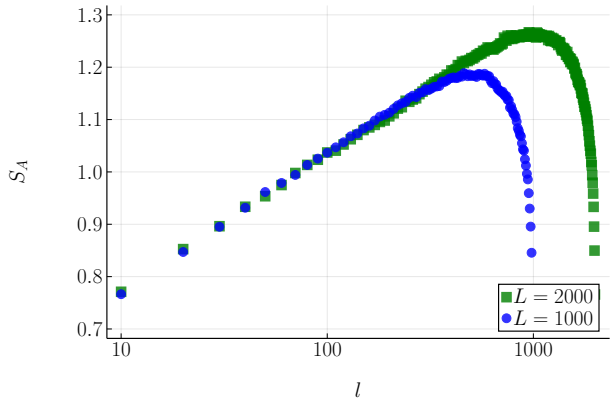

(d) Entanglement entropy of the XXX chain, no l adjustment, OBC

Figure 4.1: Entanglement entropy, recalculated from [4]. We measure the entanglement entropy of a subsystem of length l located in the left hand side of the the XXX chain. Each simulation is run for $50,000$ disorder realisations. 4.1a: the periodic chain with the adjusted subsystem length L_c. 4.1b: the open chain with the adjusted subsystem length L_c. 4.1c: the periodic chain with the unadjusted subsystem length l. 4.1d: the open chain with the unadjusted subsystem length l.

We run the analysis for $L = 1000$ and $L = 2000$ for $50,000$ disorder realisations and in each case calculate the entanglement entropy from $l = 10$ to $l = L \div 2$ with an interval of 10 in between. Our results are shown in figure 4.1, with fitted curves for the adjusted l. As can be seen in all four subfigures of figure 4.1, entropy scales logarithmically with the subsystem size. This is clearly an area law violation, and perfectly follows the prediction in [3].

These analytic predictions are accurate for $l \leq L \div 2$, after which finite size effects begin to dominate. For the periodic case the finite size effects are smaller, and can be corrected with the following two maps:

$$\ell \to L_c \equiv \frac{L}{\pi} Y\left(\frac{\pi \ell}{L}\right) \tag{4.7}$$

$$Y(x) = \sin(x)\left(1 + \frac{4}{3}k_1 \sin^2(x)\right) \tag{4.8}$$

where $k_1 = 0.115$, given by [27].

4.2 Logarithmic Negativity: Analytic Results and Numerical SDRG

In this section we recalculate the logarithmic negativity as reported in [4]. We will start by reviewing the analytic prediction via the SDRG method. We note that the groundstate as described in equation 3.8 is a tensor product of singlet states, and that from section 2.2 the logarithmic negativity is additive

under the tensor product. Before we go further it is useful to note that the partial transpose $\rho_{2S}^{T_2}$ of ρ_{2S} with respect to A_2 is:

$$\rho_{2S}^{T_2} = \frac{1}{2}\begin{pmatrix} 0 & 0 & 0 & -1 \\ 0 & 1 & 0 & 0 \\ 0 & 0 & 1 & 0 \\ -1 & 0 & 0 & 0 \end{pmatrix} \tag{4.9}$$

Furthermore, distinguishing between singlets which connect A to A, B to B, and A to B, we can follow [4] and describe the complete RSP as:

$$\rho_{RSP} = \bigotimes_{i=1}^{n_{A:A}} \rho_{2S} \bigotimes_{i=1}^{n_{B:B}} \rho_{2S} \bigotimes_{i=1}^{n_{A:B}} \rho_{2S} \tag{4.10}$$

We then trace over the B subsystem, leaving us with:

$$\rho_A = \bigotimes_{i=1}^{n_{A:A}} \rho_{2S} \bigotimes_{i=1}^{n_{A:B}} \rho_S \tag{4.11}$$

and after taking the partial transpose:

$$\rho_A^{T_2} = \bigotimes_{i=1}^{n_{A:A}} \rho_{2S}^{T_2} \bigotimes_{i=1}^{n_{A:B}} \rho_S^{T_2} \tag{4.12}$$

The logarithmic negativity is additive over this, and according to [4] it simplifies to:

$$\mathcal{E}_{A_1:A_2} = n_{A_1:A_2} \ln \mathrm{Tr} \left| \rho_{2S}^{T_2} (A_1 \cup A_2) \right| \tag{4.13}$$

where ρ is the density matrix of the generic singlet state. As discussed in section 2.2, the trace norm of a Hermitian matrix is just the sum of the absolute value of its eigenvalues. The eigenvalues of $\rho_{2S}^{T_2}$ are $\{-1/2, 1/2, 1/2, 1/2\}$, thus the trace norm is 2 and the logarithmic negativity of the total subsystem A is:

$$\mathcal{E}_{A_1:A_2} = n_{A_1:A_2} \ln 2 \tag{4.14}$$

This simply says that the logarithmic negativity of the subsystem is $\ln 2$ multiplied by the number of singlets shared between A_1 and A_2.

This result allows us to calculate the logarithmic negativity over one disorder realisation. Taking overages over the disorder with $\langle \cdot \rangle$, we have:

$$\langle \mathcal{E}_{A_1:A_2} \rangle = \langle n_{A_1:A_2} \rangle \ln 2 \tag{4.15}$$

In [4] an SDRG result for $\langle n_{A_1:A_2} \rangle$ is also given for two adjacent intervals of lengths l_1, l_2 as:

$$\langle n_{A_1:A_2} \rangle = \frac{1}{6} \ln \left(\frac{\ell_1 \ell_2}{\ell_1 + \ell_2} \right) \tag{4.16}$$

with results for disjoint systems also available. Combining equations 4.15 and 4.16 we get the final results for the logarithmic negativity:

$$\langle \mathcal{E}_{A_1:A_2} \rangle = \frac{\ln 2}{6} \ln \left(\frac{\ell_1 \ell_2}{\ell_1 + \ell_2} \right) \tag{4.17}$$

To verify this numerically, we calculate the logarithmic negativity of the one dimensional XXX chain as in [4] via the numerical SDRG method. Each subsystem is of length l and are extended in increments of 10 for every disorder realisation. The simulations are for the adjoint case, i.e. $r = 0$. We run our analysis on systems of $L = 1000$ and $L = 2000$ for $50,000$ disorder realisations in the OBC and PBC cases. The results can be seen in figure 4.2. In particular we have plotted the shifted negativity as defined in [4]:

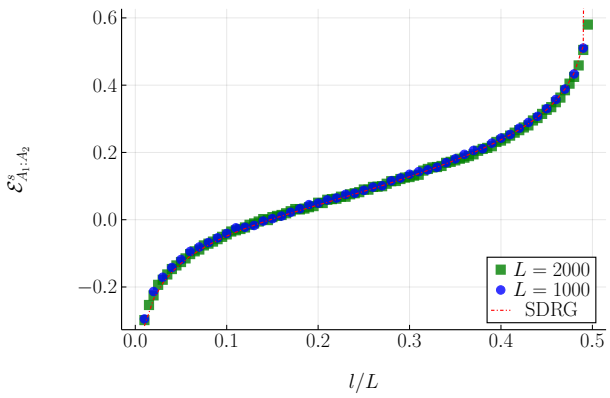

(a) Shifted logarithmic negativity as a function of l/L for the for XXX chain, $\delta = 1$, periodic boundary conditions.

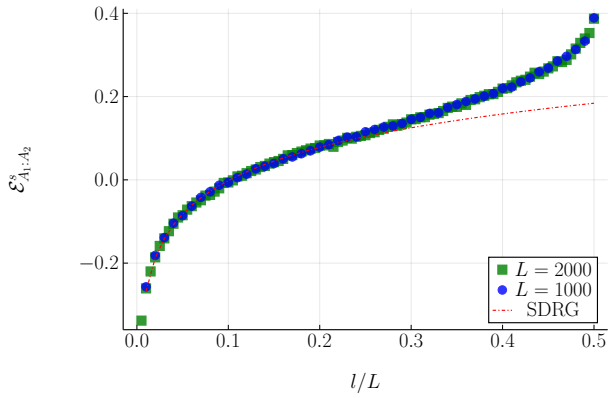

(b) Shifted logarithmic negativity as a function of l/L for the for XXX chain, $\delta = 1$, open boundary conditions.

Figure 4.2: Shifted logarithmic negativity, recalculated from [4]. In both figures, we measure the logarithmic negativity of two adjacent subsystems of length l in the XXX chain. Each simulation is run for $50,000$ trials. For implementation details, see section 4.2. 4.2a: shifted logarithmic negativity of the periodic chain with the subsystem length l. 4.2b: shifted logarithmic negativity of the open chain with the subsystem length l.

$$\mathcal{E}^s_{A_1:A_2} = \mathcal{E}_{A_1:A_2} - \frac{\ln 2}{6} \ln L \tag{4.18}$$

such that simulations for different L collapse onto the same curve. Furthermore, for the periodic case we can fit a more accurate adjusted curve as reported in [5]:

$$\mathcal{E}^s_{A_1:A_2} \simeq \frac{\ln 2}{6} \ln \frac{Y_c^2(\pi \ell/L)}{Y_c(2\pi \ell/L)} + k \tag{4.19}$$

which is an excellent fit for the periodic chain. For the open chain, we use equation 4.17, which is a good fit for $\ell/L << 1$.

To summarise the preceding sections, we have verified that for disordered models, both entanglement entropy and logarithmic negativity scale logarithmically. In the following section we will review the strongly inhomogeneous 'randbow chain'.

5 Randbow Chain: Existing Results

5.1 Entanglement Entropy: Analytic Results

In this section we move on to reproducing the results of [5], which involves modifying the couplings of the random chain to include an exponentially decaying term:

$$J_i \equiv K_i \times \begin{cases} e^{-h/2}, & i = 0 \\ e^{-h|i|}, & |i| > 0 \end{cases} \tag{5.1}$$

where the K_i terms are randomly distributed coefficients as before. This is known as the 'randbow chain'. The significance of these random couplings is to enforce a *rainbow* phase for $\lim h \to \infty$ [6] - see figure 5.1 for an illustration - which brings about a volume law scaling for the entanglement entropy. This is because for any subsystem l, the subsystem of size $l+1$ must contain another singlet link. For example, if our subsystem A starts as $A = \{J_1\}$ and we extend it to $A = \{J_1, J_2\}$, these two subsystems have 1 and 2 singlet links in them respectively, and this holds for every other subsystem up to the maximum for $l = L \div 2$. Note that if we position the subsystem centrally in the chain, then the entanglement entropy will tend to zero for the strong h phase as we only have 'complete singlets' in our subsystem (see [6] for an illustration, figure 2(b)).

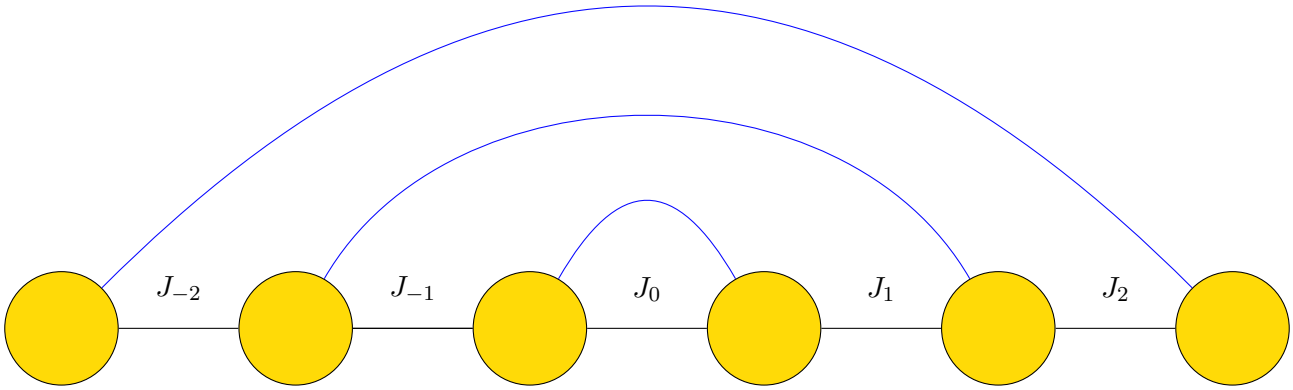

Figure 5.1: A rainbow chain as introduced in [6] and [5]. The central coupling J_0 is by definition the strongest coupling for the clean chain or for sufficiently large h, so it will always be eliminated first. The black lines represent the couplings $\{J_i\}$, whereas the blue lines represent the singlet links. Note that for the rainbow chain to make sense, we must have an odd number of links and an even number of spins in the open chain, hence the asymmetry in the diagram.

For the $h = 0$ phase we recover the random chain and the results from section 4.1 hold. However, for intermediate h the volume law does not hold. To derive the correct scaling of the entanglement entropy in this 'randbow' phase, we follow [5] and perform some intermediate analysis of the RSPs produced by SDRG in these conditions. We consider the probability distributions of the sizes of the 'rainbow' regions where spins are linked consecutively to spins more than one spin away, and 'bubble' regions where spins are linked to one of their adjacent neighbours. In any given realisation of the randbow chain, there will be continuous subregions of rainbow links and continuous subregions of bubbles (see figure 5.2 for an example).

We denote $P_r(l)$ the probability mass of seeing a rainbow subregion of length l, and similarly $P_b(l)$ for the probability of a bubble subregion of length l. We calculate these via SDRG simulation and report the results in figures 5.3a and 5.3b respectively, both with disorder parameter $\delta = 1$ and for a system size $L = 1000$ in the XX chain. We observe that for the rainbow distribution P_r, the probability of a region of length l decays exponentially in l, and that the rate of decay depends on h. However, for the P_b distribution, we observe a much slower power law decay, implying that there is no characteristic size of a bubble region, and furthermore that this does not depend on h at a scale visible on the plot.

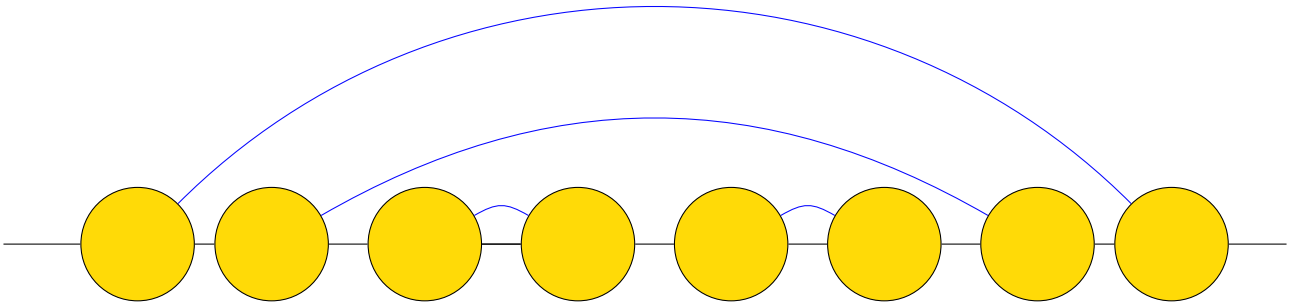

Figure 5.2: A demonstration of the bubble and rainbow subregions as named in [5]. The first two spins represent a randbow region of $l = 2$, and the second four spins represent a bubble region of $l = 4$.

This leads to an argument that the scaling of the entanglement entropy scales as a square root for the randbow chain. The argument below is slightly adapted from that given in [5], where a full analytic result is available. First, we observe from figure 5.3b that $P_b(l) \approx l^{-3/2}$, and thus:

$$\langle l_b \rangle = \int_2^l dl l P_b(l) \propto l^{1/2} \tag{5.2}$$

To a crude approximation, the number of bubble regions N_b should be equal to the number of rainbow regions N_r. Furthermore, dividing the total subsystem length l by the average length of a bubble region $\langle l_b \rangle$ gives N_b, and thus:

$$\frac{l}{\langle l_b \rangle} \propto N_b = N_r \tag{5.3}$$

The entanglement entropy is equal to the number of rainbow links in the subsystem multiplied by $\ln 2$, which is equal to the number of rainbow regions multiplied by the average length of a rainbow region:

$$S_A \propto N_r \times \langle l_r \rangle \times \ln 2 \tag{5.4}$$

Bringing together equations 5.3 and 5.4, we get:

$$S_A \propto \frac{l}{\langle l_b \rangle} \times \langle l_r \rangle \times \ln 2 \propto l^{1/2} \langle l_r \rangle \ln 2 \tag{5.5}$$

which suggests that the entanglement entropy scales as a square root, i.e. a power-law.

5.2 Entanglement Entropy: Numerical SDRG

We then verify this numerically with the SDRG as per [5] by running the SDRG procedure on the XX chain. For each simulation, we draw L random couplings from the uniform distribution over $[0, 1]$ and run the SDRG procedure for different parameters h and δ over $50,000$ disorder realisations. We present our results in figure 5.4. As h increases, the scaling of the entropy gets closer to the volume law phase, as the effect of the 'rainbow' dominates. As we approach $h = 0$, the effect is weaker and we approach the random phase again. We see that a square root scaling holds, again indicating a violation of the area law.

When we measure the entropy scaling for set ratios of h/δ, we observe a data collapse as first reported in [5]. The absolute values of h and δ no longer determine entanglement entropy but rather their ratio, with higher ratios leading to higher values of entanglement entropy. This is interestingly only in the case of the SDRG procedure and does not hold in the exact solution for the XX chain (see section 5.3).

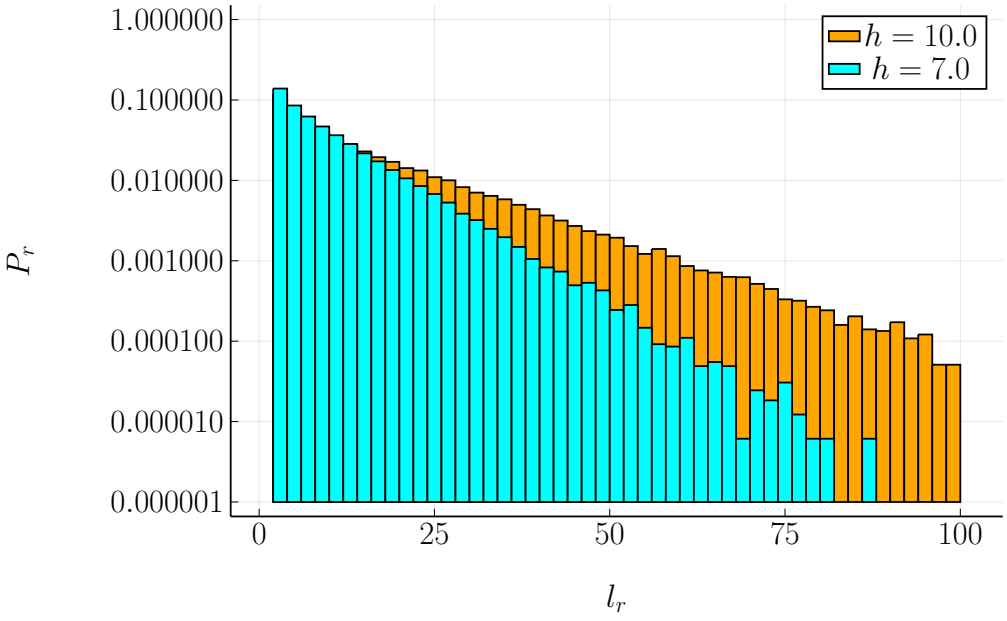

(a) Probability density function $P_r(l)$ of the lengths of rainbow subsystems. The data were collected by averaging over $10,000$ disorder realisations for $h = 10$ and $h = 7$ in the open XX chain, solved with the SDRG method. Notice the logarithmic scale on the y-axis only, suggesting an exponential decay.

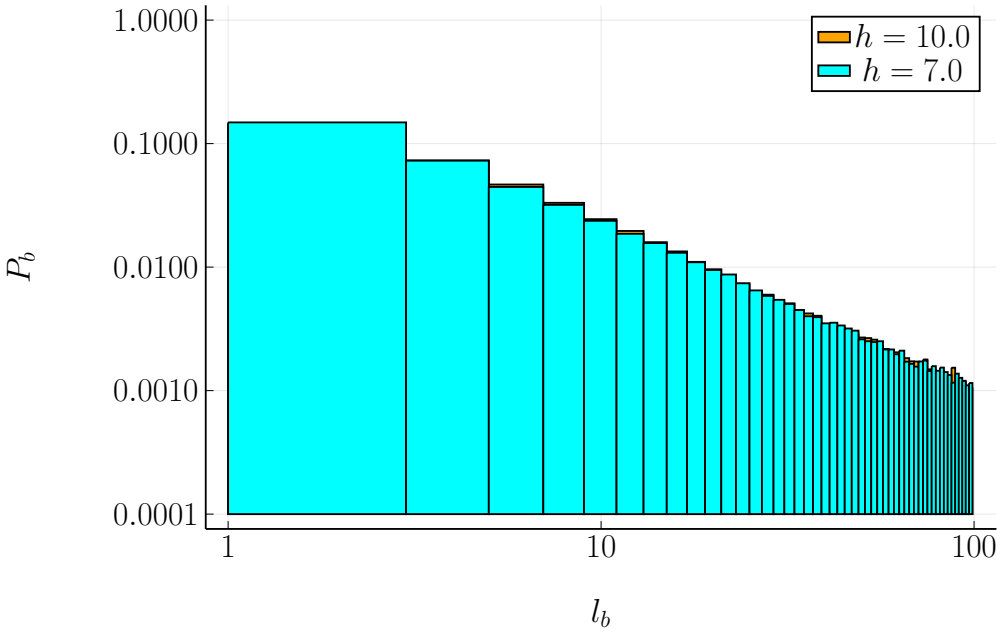

(b) Probability density function $P_b(l)$ of the lengths of bubble subsystems. The data were collected by averaging over $10,000$ disorder realisations for $h = 10$ and $h = 7$ in the open XX chain, solved with the SDRG method. Notice the logarithmic scale on both axes, suggesting a power law decay.

Figure 5.3: Subregion analysis for the XX chain of $L = 1000$. In both figures, $\delta = 1$. 5.3a: probability mass for rainbow region lengths. 5.3b: probability mass for bubble region lengths.

5.3 Randbow Chain Exact Solution

Finally, we analyse the exact solution of the XX chain. This possible in the XX case thanks to the Jordan-Wigner transformation, which maps the original $2^L \times 2^L$ eigenproblem to a much reduced $L \times L$ problem. We present the details in section A.3, and here present only the numerical findings.

We calculate the exact solution to the XX randbow chain for a system with $L = 100$ spins. We take an average over $1,000$ disorder realisations for each system and calculate the entanglement entropy from $l = 1$ to $l = 32$ for each realisation. For accuracy these simulations were run with 128-bit floating point numbers, which slows down the computation significantly as most optimised linear algebra

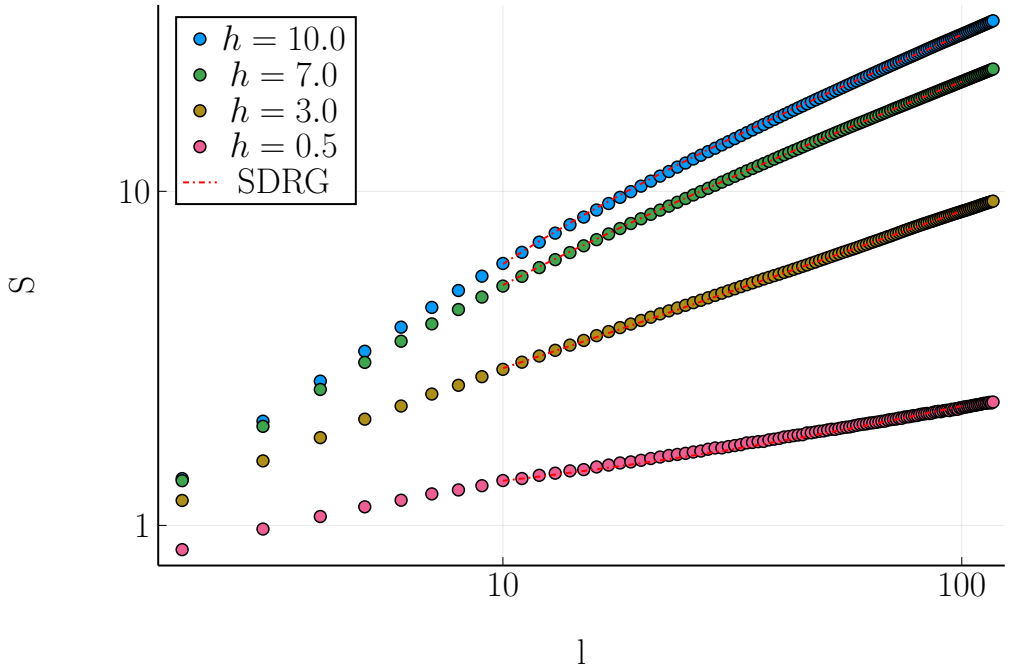

(a) Entanglement entropy for the open XX randbow chain whilst varying the exponential parameter h. Notice the log-log scaling on each axis. Each simulation is run for $50,000$ disorder realisations, and we measure the entanglement entropy of a subsystem A starting at the chain centre for each realisation. A fitted function of the form $y = a + b\sqrt{x}$ is overlayed for each value of h.

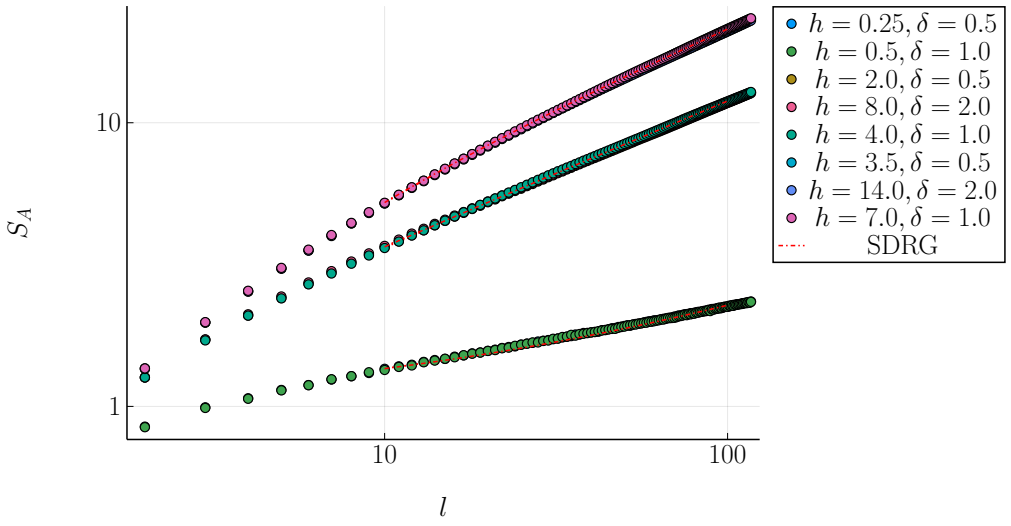

(b) Entanglement entropy for the open XX randbow chain whilst varying the exponential parameter h and the disorder parameter δ in fixed ratios. Again, notice the log-log scaling on each axis. Each simulation is run for $50,000$ disorder realisations, and we measure the entanglement entropy of a subsystem A starting at the chain centre for each realisation. A fitted function of the form $y = a + b\sqrt{x}$ is overlayed for each value of h/δ.

Figure 5.4: Entanglement entropy scaling of the randbow chain via SDRG. 5.4a: the entanglement entropy scales as a square root. Figure 5.4b: data collapse onto h/δ.

routines are designed for 64-bit precision or lower. The results for the disordered cases are shown in figure 5.5a. Note the $\log_2$ scaling on each axis. The entanglement entropy retains its clear square root scaling, but we observe the the data collapse onto the h/δ ratios is no longer present. In addition, the absolute increase in h does increase the entanglement entropy at all scales l.

Furthermore, we calculate the entanglement entropy of the clean rainbow chain, and our results are in figure 5.5b. Here we see the volume law very clearly, even for relatively weak inhomogeneity $h = 1.5$.

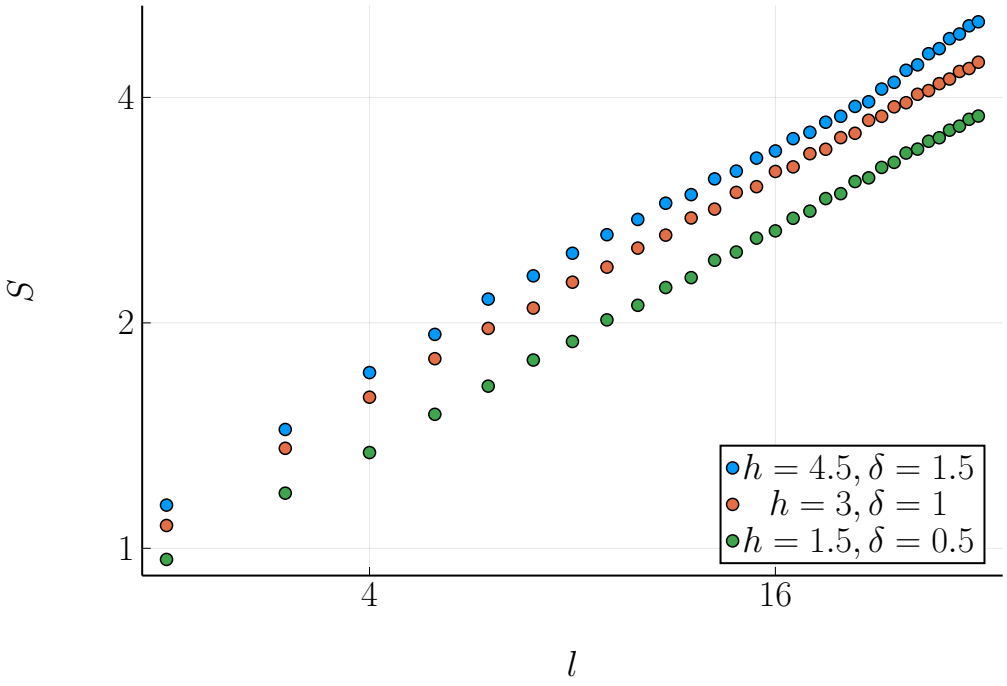

(a) Entanglement entropy scaling of the XX randbow chain with the exact solution. We calculate the solution for the $L = 100$ chain with $\delta = 1$ for $1,000$ disorder realisations. Notice the logarithmic scales on both axis, and that the data collapse on the ratio h/δ is no longer present.

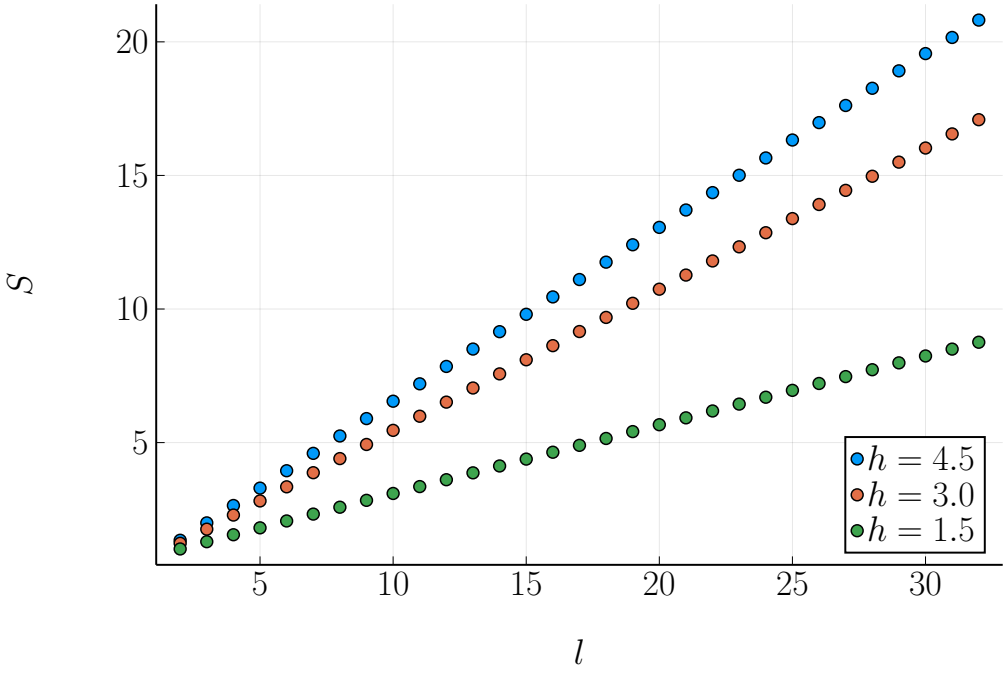

(b) Scaling of the entanglement entropy of the clean open XX chain, calculated with the exact solution to the groundstate problem with varying h on a system of size $L = 100$, with $\delta = 0$. Notice the volume scaling in l.

Figure 5.5: Entanglement entropy scaling of the randbow chain with the exact solution. We calculate the solution for the $L = 100$ chain. 5.5a: the exact solutions for the XX chain with disorder ($\delta = 1$) for $1,000$ disorder realisations. Figure 5.5b: the exact solution of the clean case.

6 Logarithmic Negativity for the Randbow Chain

6.1 Analytical Expectation

In the following sections, we begin our extension of the existing results. We start by analysing the logarithmic negativity an open randbow chain with two adjacent intervals as we vary the subsystem length l. This simulation setup is identical to that seen in 3.2, except that we use the randbow couplings rather than the basic disordered couplings.

For the $h \to \infty$ limit, we would expect the negativity to follow the volume law. The argument is essentially the same as that made for the large h entanglement entropy: for every extra spin in A_1, we introduce another singlet link between A_1 and A_2, thus we get a volume law.

For moderate values of h, we can predict a power-law scaling via a very similar argument to that presented in 5.1. First, recall that the logarithmic negativity in the RSP is the number of singlet links between the two subsystems, multiplied by $\ln 2$. Secondly, assume that all of the singlet links coming *out* of A_2 go into A_1, and vice versa. This allows us to reduce the problem to just calculating the scaling of the entanglement entropy of either of the subsystems, which is just the number of singlet links connecting outside of the subsystem (A_1 or A_2 here). We have already shown that the entanglement entropy for the randbow chain scales with a power-law, which suggests that the logarithmic negativity will also scale as a power-law. This is valid in as far as the approximation that all of the singlet links coming *out* of A_2 go into A_1 is accurate.

It is important to point out that this argument, based on that given in [5], only holds in the non-interacting case. We will see in the numerical evidence that this is indeed the case and the interacting model shows a saturating behaviour consistent with [5].

6.2 Numerical SDRG

To verify these results, we measure the logarithmic negativity of two adjoint subsystems in the XX and XXX randbow chains with the numerical SDRG method, with $L = 1000$ and 2000 in both cases. We use the SDRG procedure for $50,000$ disorder realisations each, and plot the logarithmic negativity as a function of the adjusted subsystem length l/L. In both cases we use the parameters $h = 1, \delta = 1$ for the moderate inhomogeneity regime. Our results are shown in figure 6.1.

As can be seen from figure 6.1a, in the XX case the square root scaling is well captured. In the XXX model, we observe the same saturation behaviour reported for the entanglement entropy in [5]. This is to be expected given the the argument made above in section 6.1: to calculate the logarithmic negativity we only need to know the entanglement entropy, and we already expect this to saturate in l.

As an additional measure of the rate at which entanglement decays from the centre of the chain, we measure the logarithmic negativity as we vary the interval r between two adjacent intervals in the XX and XXX chains. We consider only even r, with the interval spaced evenly over the centre of the chain (see figure 3.2 for a visualisation) with $L = 1000$. We observe that in the XX case, the logarithmic negativity decays relatively slowly as r increases. This is to be expected given the previously discussed stability of the rainbow regions in the XX case relative to the bubble regions. Furthermore, we notice a strong data collapse onto the ratios h/δ, just as for the previous measures of entanglement.

However, in the interacting XXX case, the logarithmic negativity decays far more quickly, as expected from the saturating behaviour we see in figure 6.1b. This is a corollary of figure 6.1b: as we extend into the extremes of the chain, we see fewer long distance singlet connections.

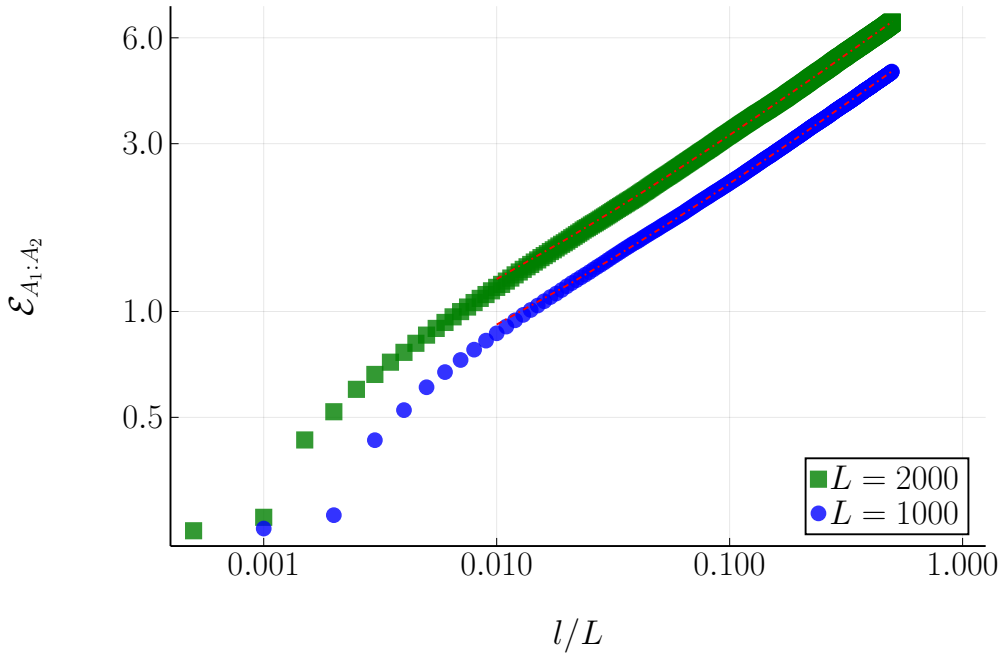

(a) Logarithmic negativity for the open randbow XX chain. Notice the logarithmic scale on both axes. The fitted curve is of the form $a + b\sqrt{x}$.

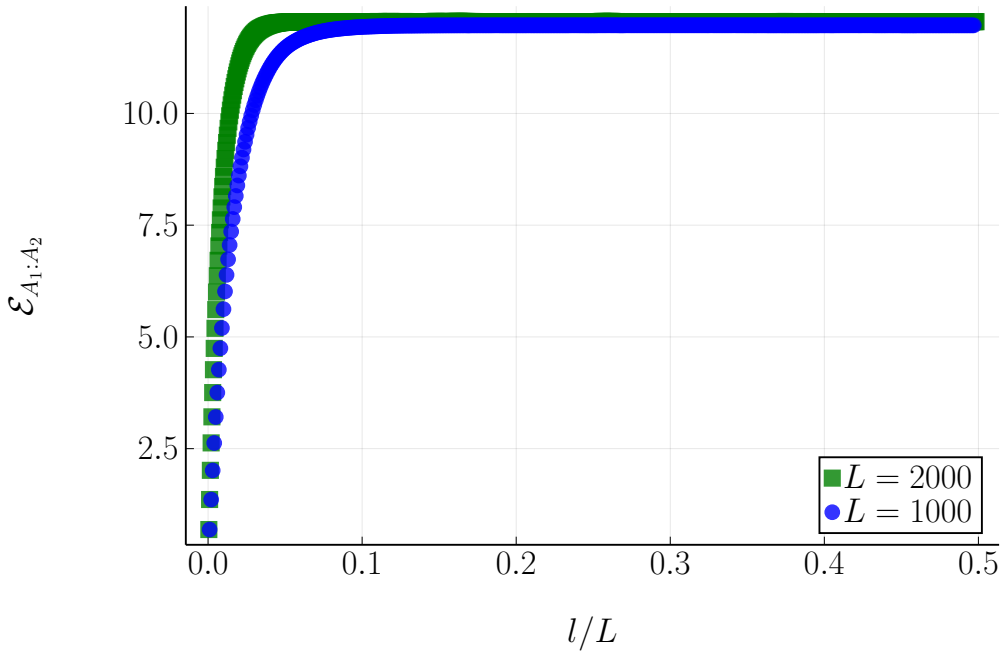

(b) Logarithmic negativity for the open randbow XXX chain. Notice the rapid saturation, indicative of an area law.

Figure 6.1: Logarithmic negativity scaling in the open randbow chain for adjoint subsystems. We set $h = 1, \delta = 1, L = 100$ in both figures and measure the logarithmic negativity over $50,000$ disorder realisations. We place the subsystems A_1 and A_2 in the centre of the chain. In both figures we run the simulation for $L = 1000$ and $L = 2000$. 6.1a: scaling in the XX regime. A square root scaling is observed, reflecting analytical expectations and the results from 5.3. 6.1b: scaling in the XXX regime. We observe that the logarithmic negativity saturates quickly in both system lengths.

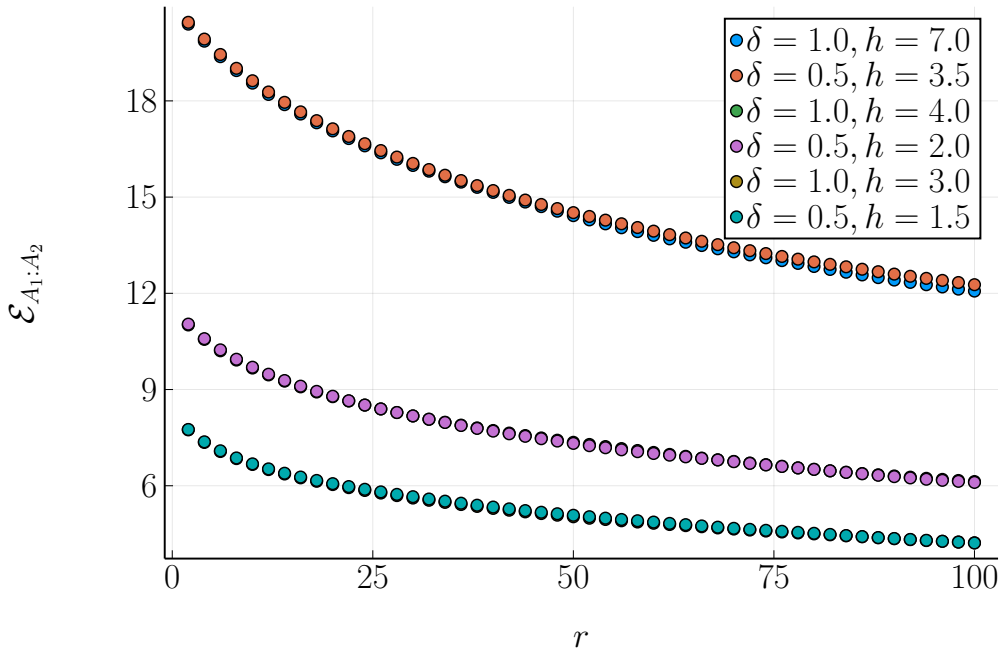

(a) Logarithmic negativity in the XX randbow with varied interval r, OBC

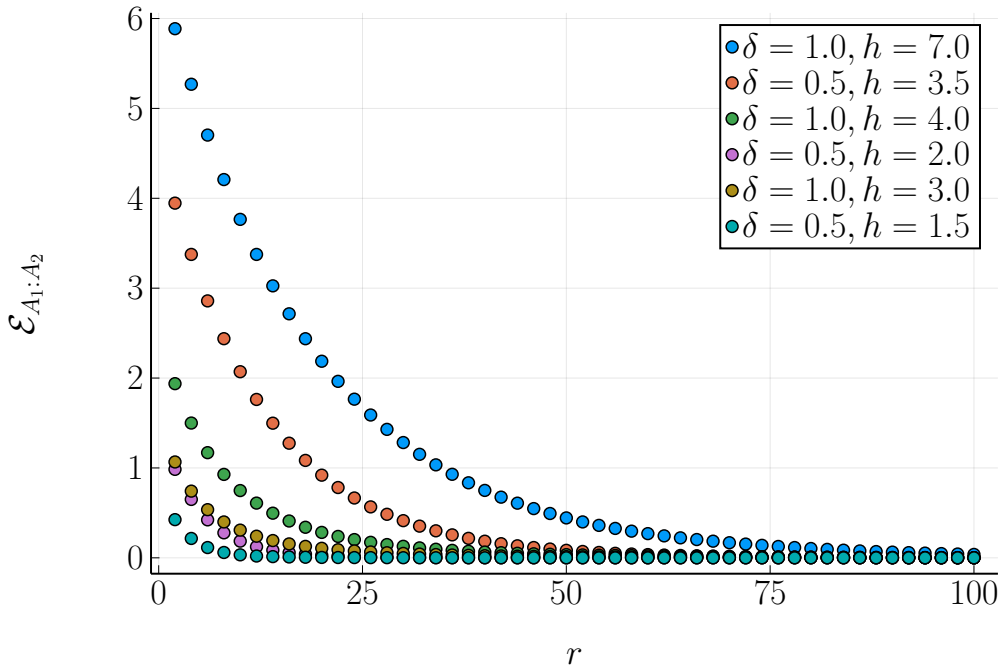

(b) Logarithmic negativity in the XXX randbow with varied interval r, OBC

Figure 6.2: Logarithmic negativity scaling in the randbow chain for disjoint subsystems as we vary r. We measure the logarithmic negativity over $50,000$ disorder realisations. We place the subsystems A_1 and A_2 in the centre of the chain separated by an even interval r, located in the centre of the chain. $L = 1000$ and $l = 100$ in both figures. 6.2a: the XX chain. The logarithmic negativity decays relatively slowly, in line with figure 6.1a. We also observe a strong data collapse onto the ratio h/δ. 6.2b: scaling in the XXX model. The logarithmic negativity decays much more quickly, in line with figure 6.1b, and there is no observable data collapse other than the $r \to 0$ limit in which all entanglement is lost.

7 Power-Law Spin Chains

In [6], it is mentioned that the couplings must decay quickly for the rainbow chain to be enforced. In particular they suggest that:

$$J_i = \mathcal{E}^{\alpha(i)} \tag{7.1}$$

where $\alpha(i)$ is monotonically decreasing. To explore how sensitive the scaling of entanglement is to the speed of this decay, we consider a new power-law spin chain with couplings given by:

$$J_i \equiv K_i \times \begin{cases} 2, & i = 0 \\ |i|^{-\alpha}, & |i| > 0 \end{cases} \tag{7.2}$$

In the case where $i = 0$, i.e. when we are determining the central coupling, we have chosen 2 as the second factor to ensure that the total function $F(i)$ (see equation 3.2) is peaked at i.

7.1 Analytic Results

In [5], it is possible to derive analytic expectations for the randbow chain only in the strongly inhomogeneous limit $h \to \infty$ (see in particular section VI.A). This is because only in the limit (and with symmetric J_i) can we be sure that the central bond will always be eliminated first and that the elimination process will be symmetric with respect to the chain.

Unfortunately, for the power-law spin chain, we cannot guarantee that the central bond will be eliminated first, nor that the process will be symmetric. The reason is that the effect of the power-law component is not enough, relative to the effect of the $\mathcal{O}(1)$ disorder factor, to rapidly reduce the consecutive couplings. Given that, as discussed in section 3.3, the elimination rule always reduces the energy scale, the couplings around the elimination site must be small enough to still be smaller than the new J' coupling. In the power-law spin chain, this cannot be guaranteed to be the case.

As such, we will investigate the empirical scaling of the entanglement entropy and logarithmic negativity in these power-law spin chains via numerical SDRG in sections 7.2 and 7.3. Lastly, in section 7.4, we will explore some possible explanations for our findings.

7.2 Entanglement Entropy: SDRG and exact results

We start by calculating the scaling of the entanglement entropy of the open XX power-law spin chain with the numerical SDRG method for $L = 1000$ and $L = 2000$. We use $\delta = 1$ in all of these simulations. We run all of the simulations for $50,000$ disorder realisations and the results are shown in figure 7.1.

In both figures, we can see that the entanglement entropy scales similarly to the simple disordered model. For low l the entanglement increases quickly, which suggests that the rainbow phase does survive for at least the first few eliminations. After the initial phase, the scaling becomes closer to the logarithmic scaling seen the in disordered model. However, we notice that the most inhomogeneous situation ($\alpha = 10$) does not correspond to the most entangled situation, in constrast to the randbow chain. This suggests that the effect of α in the power-law spin chain is not as simple as the effect of h in the randbow spin chain. Lastly, we observe some finite size effects for $l/L \approx 1/2$. We have not attempted to fit any of the analytical curves from the simple disordered model due to the very different low l region.

Furthermore, we measure the entanglement entropy via the exact solution. Over 1000 disorder realisations, we calculate the entanglement entropy of the XX power-law spin chain for an open chain of length 100. Our results are shown in figure 7.2. This is a close match to the low l pattern observed in figures 7.1a and 7.1b. Interestingly, we observe a strong data collapse onto the ratio α/δ that is not present in the SDRG numerics. Again, we have not fitted any predictions from the disordered model as the scaling is not exactly logarithmic.

7.3 Logarithmic Negativity Scaling: SDRG

In this section, we look at the logarithmic negativity of the power-law spin chain. Specifically we measure the logarithmic negativity of the open XX and XXX power-law spin chains for $L = 1000$ and $L = 2000$. We run each simulation for $50,000$ disorder realisations, and our results are shown in 7.3.

For both values of L, we observe that the scaling appears very similar to the simple disordered chain. For low l/L the scaling appears logarithmic before increasing as we approach half of the chain. Interestingly, the curve for $L = 2000$ is higher in both the XX and the XXX simulations than the $L = 1000$ curve. This may be explained by the presence of some persistent rainbow regions even in the power-law model: half of the $L = 2000$ rainbow chain will contain more singlet links between the two subsystems than a subsystem of the same relative size for $L = 1000$.

Finally, we calculate the scaling of the logarithmic negativity for a varying interval r between two subsystems, in a manner identical to that discussed in 6.2. Our results for the open XX and XXX chains with disorder $\delta = 1$ are reported in figure 7.4. We observe that the logarithmic negativity decays much more quickly than in the randbow chain, which we might expect given the relative instability of the rainbow regions. We do not observe the data collapse shown in figure 7.4a for the non-interacting randbow chain, which again suggests the the system behaviour is qualitatively different.

7.4 Possible explanations

Whilst we cannot make any rigorous predictions about the entanglement scaling for the power-law spin chain, after observing the data we can make some conjectures about the qualitative behaviour. Given that we do not expect the couplings to decay quickly enough to maintain a rainbow phase, we might expect that the power-law spin chain will behave at least asymptotically as the simple disordered system. This suggests the following hypotheses:

1. The entanglement entropy will scale in a manner similar to the simple disordered spin chain as seen in section 4.1.

2. The logarithmic negativity will also scale in a manner similar to the simple disordered spin chain as seen in section 4.2.

Again, we do not have any rigorous proof of these hypotheses, but they do corroborate the simulation data well.

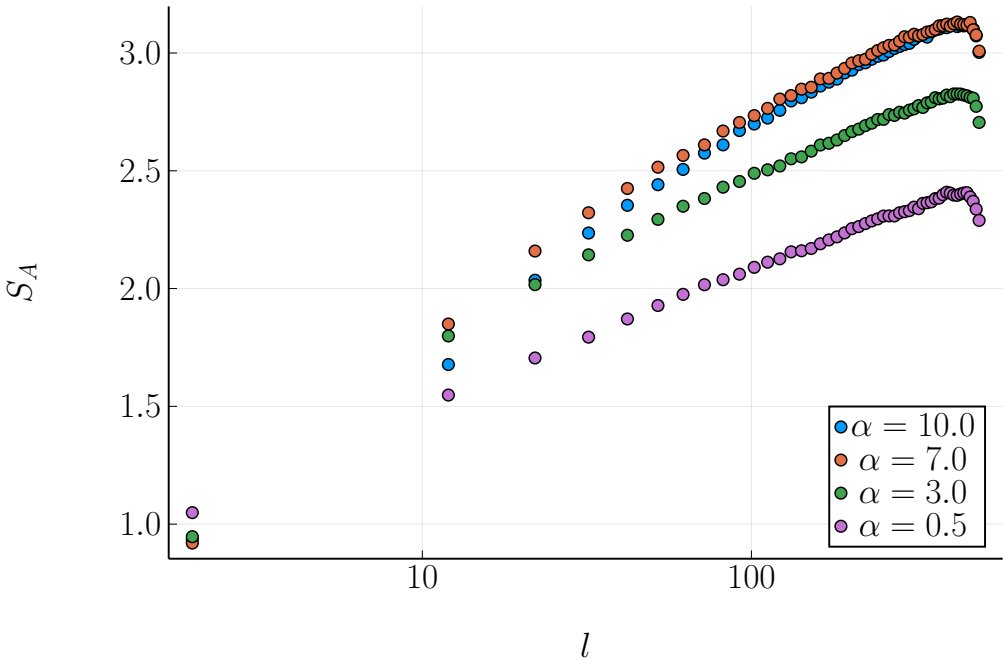

(a) Entanglement entropy of the XX power-law spin chain via SDRG for $L = 1000$, varying α, OBC. Notice that the entanglement scales similarly to the simple disordered model.

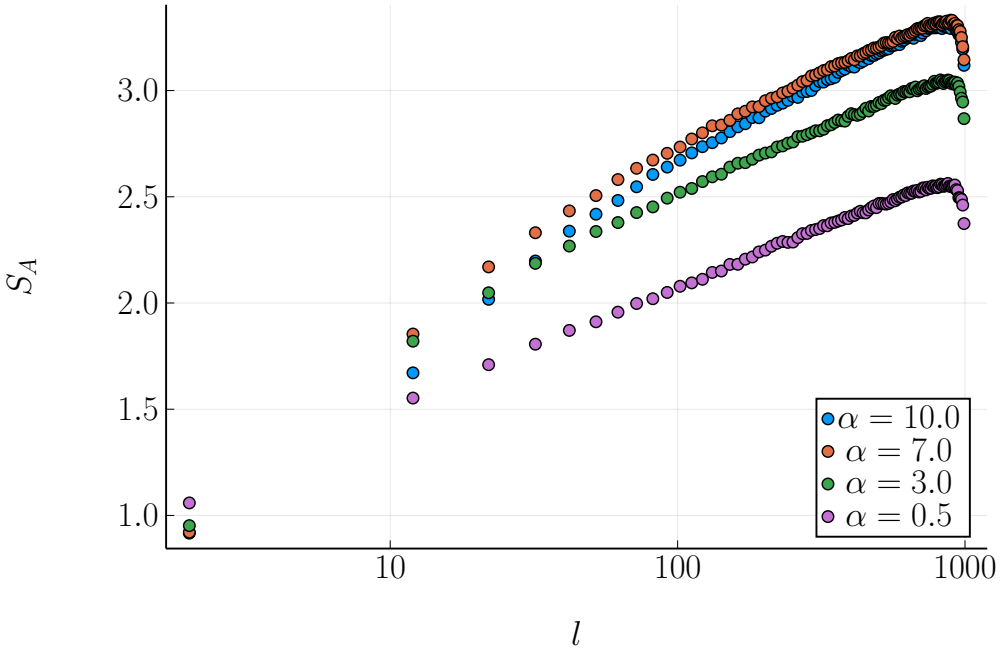

(b) Entanglement entropy of the XX power-law spin chain via SDRG for $L = 2000$, varying α, OBC. Notice that the entanglement scales similarly to the simple disordered model.

Figure 7.1: Entanglement entropy for the open XX power-law spin chain, calculated via the SDRG method for $L = 1000$ and 2000. In both figures, we calculated the entropy of a subsystem A over $50,000$ disorder realisations. For each system size we ran the simulation with a different parameter α and with $\delta = 1$. Figure 7.1a: $L = 1000$. Figure 7.1b: $L = 2000$.

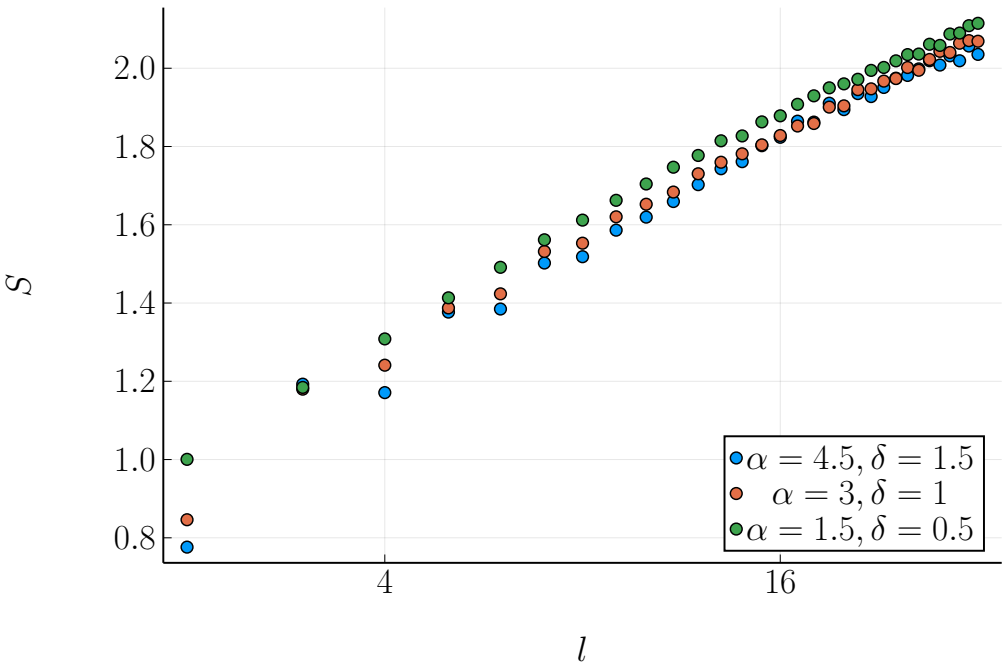

Figure 7.2: Entanglement entropy of the open XX power-law spin chain, calculated with the exact solution over $1,000$ disorder realisations with $\delta = 1$. For each simulation we vary α and $\delta = 1$. The system length is $L = 100$.

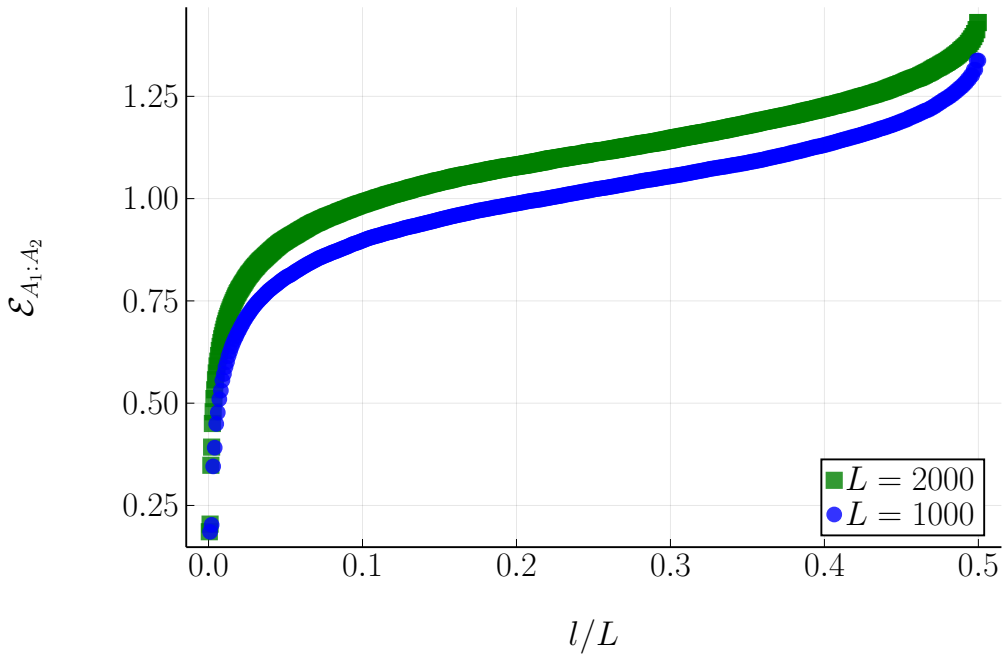

(a) Scaling of the logarithmic negativity in the power-law spin chain, XX, OBC

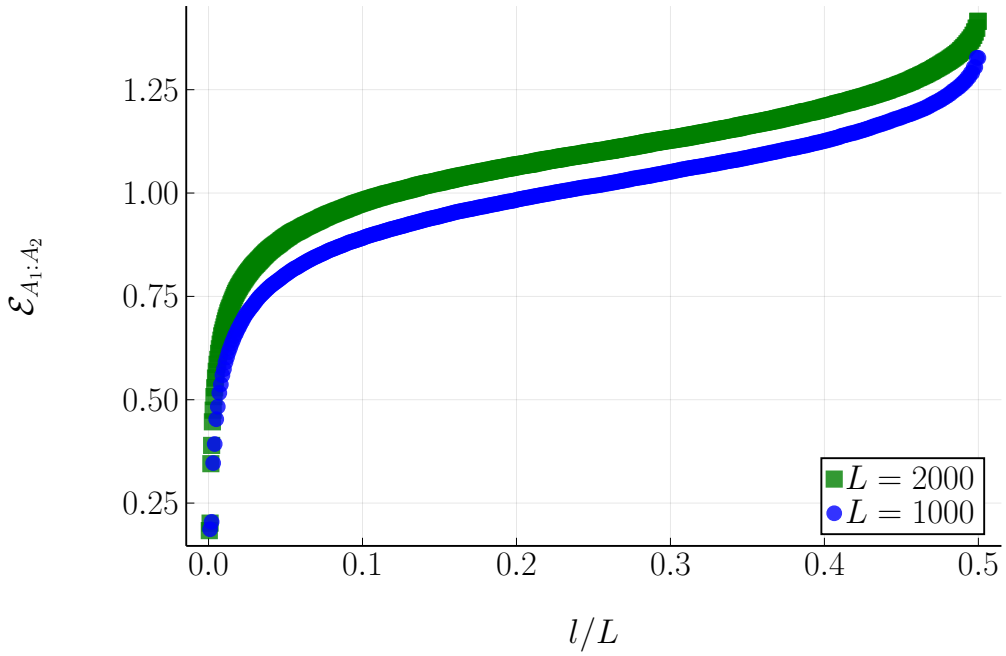

(b) Scaling of the logarithmic negativity in the power-law spin chain, XXX, OBC

Figure 7.3: Scaling of the logarithmic negativity of the open power-law spin chain. In each figure we calculate the negativity over $50,000$ disorder realisations whilst keeping $\alpha = 1, \delta = 1$. 7.3a: logarithmic negativity for the XX chain. 7.3b: logarithmic negativity for the XXX chain. Notice that in each subfigure, the $L = 2000$ curve is shifted upwards relative to the $L = 1000$ curve.

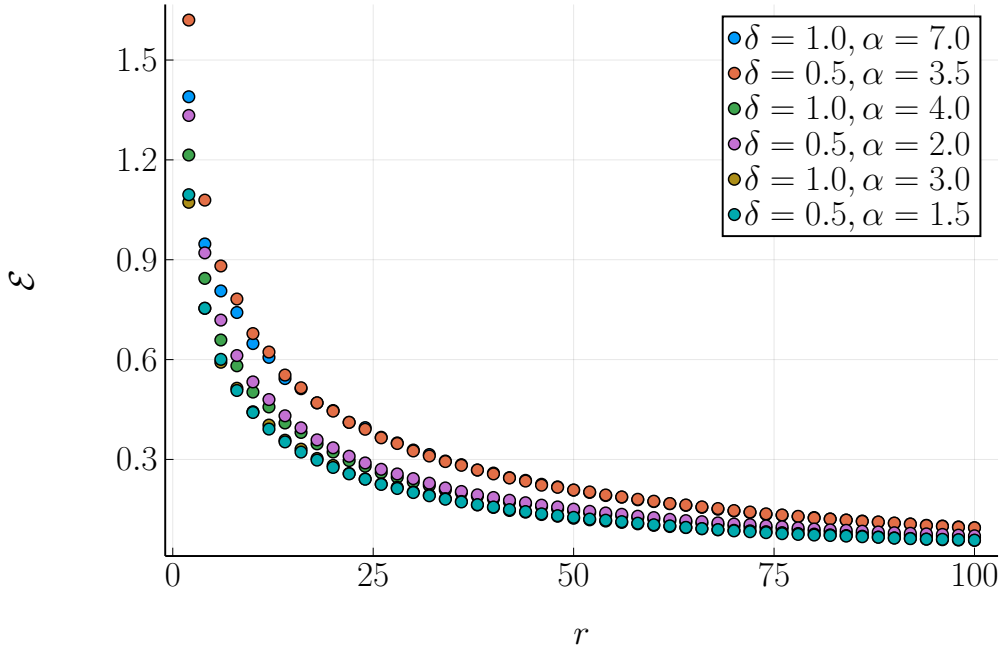

(a) Logarithmic negativity in the power-law spin chain with varying r, XX, OBC. Notice in this case that there is a data collapse onto the ratio α/δ.

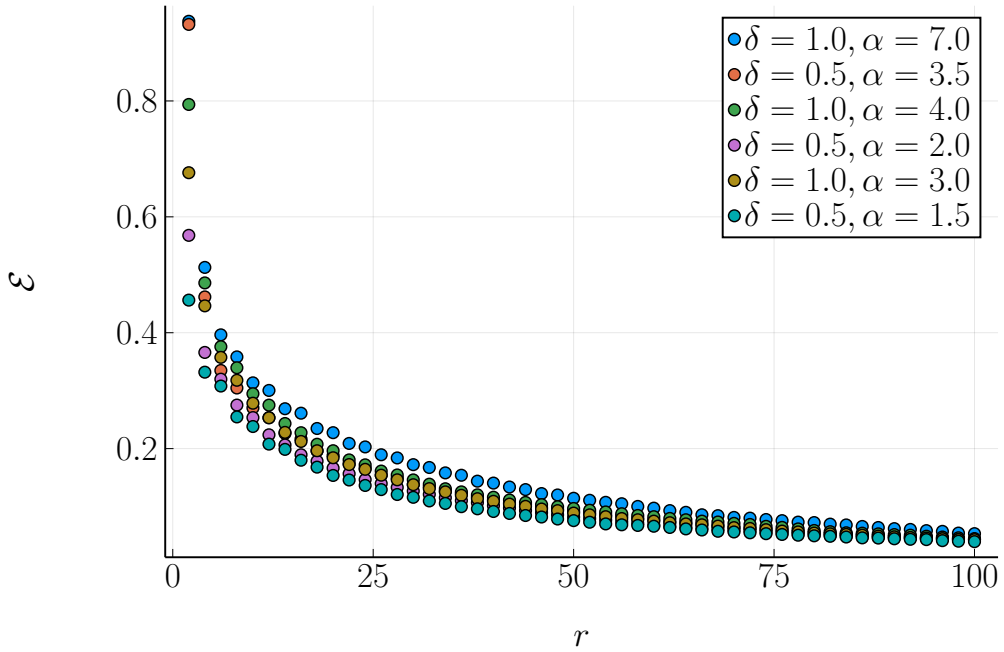

(b) Logarithmic negativity in the power-law spin chain with varying r, XXX ($\Delta = 1$), OBC. Notice in this case that there is no obvious data collapse.

Figure 7.4: Scaling of the logarithmic negativity of the open XX and XXX power-law spin chains as r is varied. We restrict r to even intervals and the position is the same as per figure 6.2. $L = 1000$ and $l = 100$ in both figures. We notice that the logarithmic negativity decays very quickly compared to the non-interacting randbow case, figure 6.2a.

8 Conclusion

In this report we have confirmed some key findings in the literature on entanglement scaling in random spin chains, as well as exploring new measures and new systems. In section 6 we showed with a simple proof that the scaling of the logarithmic negativity of the randbow chain should be similar to the scaling of the entanglement entropy. We verified this via the numerical SDRG method. In the non-interacting, XX case, we observed a power-law scaling, and for the interacting XXX case, we saw that the entanglement entropy quickly saturated, which reflects the stability of the bubble regions in this regime. We similarly noted that for fixed subsystem sizes but increasing intervals r, the negativity of the interacting model scaled far more quickly than the non-interacting model, which is a corollary of the previous result.

For a system with couplings distributed according to a power-law, we were not able to derive any exact results. However, the scaling of the entanglement entropy and the logarithmic negativity computed via the numerical SDRG method changed significantly compared to the randbow model. Our numerical observations suggest that it does not maintain the square root entanglement scaling of the randbow chain, despite the inhomogeneous factor in the spin couplings. The entanglement entropy at first scaled quickly with l, suggesting that a short rainbow phase dominates. However, this rainbow phase appeared to be very unstable, likely due to the relatively slow decaying of the couplings, and from that point onwards the scaling appeared to be logarithmic. This was corroborated with the scaling of the exact case for a smaller system size. Similarly for the logarithmic negativity, we observed via the numerical SDRG method that the power-law spin chain scales as expected in a very similar way to the simple disordered system.

Whilst we were not able to establish any analytical results for the power-law spin chain, this could be achieved more time. One issues is that the power-law expression is not as analytically malleable as the exponential expression, so any solution will probably not take the same form as the details of [5].

A more exhaustive treatment could have been made of the different ways of measuring the entanglement entropy and logarithmic negativity of the power-law spin chain - for example, calculating the exact solution for the entanglement entropy calculations for a different value of α/δ. Similarly, given more compute power it would have been interesting to calculate the exact solution for both the randbow chain and the power-law chain for l up to $2,000$. Furthermore, we have not considered values of Δ outside of 0 and 1. Lastly, we attempted to investigate whether the power-law scaling of the entanglement entropy would hold in the power-law spin chain with very high α (including $\alpha = 500$) but these results were inconclusive. All of the above points could be the subject of future work.

A Quantum Mechanics and the Jordan-Wigner Transformation

Quantum mechanics is built on state vectors that have a different notion of state to classical state vectors. In a classical system, a state $s(t)$ at time t provides all of the information needed to predict the outcome of an experiment if the experiment were conducted at time t. The mapping of moments in time to possible experimental outcomes is one to one. To have information about the state of a system means that you know what result you will get if you observe the system.

However, in quantum mechanics, the mapping of states to possible experimental outcomes is one to many. A quantum state does not, in general, tell us what we will observe at t - rather, it encodes a range of possible observations that could be made when the experiment happens. The result of the experiment will not be known until the experiment has taken place.

In this section we will briefly summarise the quantum mechanical formalism used throughout the paper, and in particular some details of the Jordan-Wigner transformation as used in 5.3 and 7.2. We will assume the reader is familiar with bra-ket notation and understands the general idea of an operator as it is used in quantum mechanics. For an excellent introduction, see [28].

A.1 Commutators

Most operators do not commute, and the same is true within quantum mechanics. We define the *commutator*:

$$[A, B] = AB - BA \tag{A.1}$$

The *anti-commutator* is defined as:

$$\{A, B\} = AB + BA \tag{A.2}$$

Commutation relations are important in defining the relationships between operators. For example, given the position operators $\hat{x}$ and the momentum operator $\hat{p}$:

$$[\hat{x}, \hat{p}] = i\hbar\mathbb{I} \tag{A.3}$$

This relation between two operators that are Fourier transforms of one another is often referred to as the canonical commutation relation.

A.2 Spin

Spin is a form of angular momentum inherent to quantum particles characterised by a *spin quantum number* s. Restrictions on this spin quantum number imply important properties about different quantum particles. Spin is quantised and takes the form:

$$S = \hbar\sqrt{s(s+1)} \tag{A.4}$$

where s can be any half-integer. Particles with half-integer spin are *fermions* and particles with integer spins are called *bosons*.

An important property of fermions is that they obey the Pauli Exclusion Principle [29]. Consider a creation operator $a_i^\dagger$ that acts on a vacuum state $|0\rangle$ to create a particle at position i[3]. Adding a particle at position i and another at position j must give us the same state, up to a prefactor:

$$a_i^\dagger a_j^\dagger = \lambda a_j^\dagger a_i^\dagger \tag{A.5}$$

Restricting ourselves without loss of generality to the cases ± 1, we consider the bosonic case of $+1$ first, which implies that the state vector is symmetric under particle exchange. This also implies that:

[3]This explanation of the exclusion principle is due to Blundell and Lancaster [30].

$$a_i^\dagger a_j^\dagger - a_j^\dagger a_i^\dagger = [a_i^\dagger, a_j^\dagger] = 0 \tag{A.6}$$

However, for the *fermionic* case, we have the prefactor -1 and instead the anti-commutator $\{c_i^\dagger, c_j^\dagger\} = 0$, where $c_i^\dagger$ is the fermionic creation operator at i. Mostly importantly, if we set $i = j$ then:

$$c_i^\dagger c_i^\dagger + c_i^\dagger c_i^\dagger = 0 \tag{A.7}$$

$$c_i^\dagger c_i^\dagger = 0 \tag{A.8}$$

Which is exactly the Pauli Exclusion Principle: if we try to create two fermions at the same position, they annihilate and we get nothing at all. This will be relevant when we discuss the Jordan-Wigner transformation in the following section.

A.3 The Jordan-Wigner Transformation

The Jordan-Wigner (JW) transformation maps a system of spins onto a system of (free) fermions. This is useful as it opens up a wider variety of technqiues for dealing with disordered, many body problems. We recommend [31] for a thorough overview, and our summary of the JW transformation relies heavily on their layout.

Recall from A.2 that a fermion obeys the Pauli exclusion principle and that one can define a creation operator $c_i^\dagger$ with anti-commutator $\{c_i^\dagger, c_j^\dagger\} = 0$,. Using this, the JW transformation maps spins to fermions according to the following transformations:

$$\hat{\sigma}_j^x = \hat{K}_j \left(\hat{c}_j^\dagger + \hat{c}_j\right) \tag{A.9}$$

$$\hat{\sigma}_j^y = \hat{K}_j i \left(\hat{c}_j^\dagger - \hat{c}_j\right) \tag{A.10}$$

$$\hat{\sigma}_j^z = 1 - 2\hat{n}_j \tag{A.11}$$

where $\hat{n}_j = \hat{c}_j^\dagger \hat{c}_j$ is the fermionic number operator and $\hat{K}_j = \prod_{j'=1}^{j-1} (1 - 2\hat{n}_{j'})$ is a parity adjusting operator. The physical picture here is that we have gone from spins that can be 'up or down' to fermions that can be present or not.

These mappings can be reversed, following [4]:

$$c_i = \left(\prod_{m=1}^{i-1} \sigma_m^z\right) \frac{\sigma_i^x - i\sigma_i^y}{2} \tag{A.12}$$

In the following section we show how this technique can be used to solve the random inhomogeneous chain.

A.4 Using the JW Transformation in the Exact Solution

Again following [4], we define a slightly more general Hamiltonian than equation 3.1 as follows:

$$H_{XX} = \sum_i J_i \left(S_i^x S_{i+1}^x + S_i^y S_{i+1}^y\right) + h \sum_i S_i^z \tag{A.13}$$

Note that this applies strictly to the XX chain, and the additional h term. Using equation A.12 this is immediately transformed into a fermionic form:

$$\mathcal{H}_{XX} = \frac{1}{2} \sum_{i=1}^{L-1} J_i \left(c_i^\dagger c_{i+1} + c_{i+1}^\dagger c_i\right) + \frac{h}{2} \sum_{i=1}^{L-1} c_i^\dagger c_i \tag{A.14}$$

where we have defined the additional anti-commutator relation $\left\{c_m, c_n^\dagger\right\} = \delta_{m,n}$.

One can now assume that each new fermion has individual eigenstates of the form:

$$\eta_q^\dagger|0\rangle = \sum_i \Phi_q(i) c_i^\dagger|0\rangle \tag{A.15}$$

where q labels the different eigenstates and Φ is a vector of amplitudes to be found. The Schrödinger equation becomes:

$$J_i\Phi_q(i+1) + J_{i-1}\Phi_q(i-1) = 2\epsilon_q\Phi_q(i) \tag{A.16}$$

where ϵ_q are single particle eigenvalues per eigenstates q. This is a new eigenvalue problem for a banded $2L \times 2L$ matrix with the couplings J_i on the off-diagonals.

The groundstate of the original Hamiltonian will have $L \div 2$ fermions, giving us the following:

$$|GS\rangle = \eta_{q_M}^\dagger \eta_{q_{M-1}}^\dagger \cdots \eta_{q_1}^\dagger|0\rangle \tag{A.17}$$

Multiplying equation A.15 by the relevant operators, we can derive the anti-commutators:

$$\left\{\eta_q^\dagger, c_j^\dagger\right\} = \{\eta_q, c_j\} = 0 \tag{A.18}$$

and

$$\left\{\eta_q^\dagger, c_j\right\} = \Phi_q(j)\delta_{k,j}, \quad \left\{\eta_q, c_j^\dagger\right\} = \Phi^*(j)\delta_{k,j} \tag{A.19}$$

Combining the previous two equations, we can derive the two point function's expected value for the groundstate of the original Hamiltonian:

$$\left\langle c_i^\dagger c_j \right\rangle = \sum_q \Phi_q^*(i)\Phi_q(j) \tag{A.20}$$

This defines a matrix $C_{i,j}$ that can be restricted to some subsystem A for the purposes of analysing a given disorder realisation. In particular, from [32], we can calculate the entanglement entropy:

$$S_A = -\sum_l \left(\lambda_k \ln\lambda_k + (1-\lambda_k)\ln(1-\lambda_k)\right) \tag{A.21}$$

This completes our overview of the technique used in 5.3 to calculate the entanglement entropy exactly.

References

[1] J. Eisert, M. Cramer, and M. B. Plenio. "Area Laws for the Entanglement Entropy". In: *Reviews of Modern Physics* 82.1 (Feb. 4, 2010), pp. 277–306. ISSN: 0034-6861. DOI: 10.1103/RevModPhys.82.277. arXiv: 0808.3773. URL: https://link.aps.org/doi/10.1103/RevModPhys.82.277.

[2] M. B. Hastings. "An Area Law for One Dimensional Quantum Systems". May 14, 2007. DOI: 10.1088/1742-5468/2007/08/P08024. arXiv: 0705.2024. URL: http://arxiv.org/abs/0705.2024 (visited on 08/18/2022).

[3] G. Refael and J. E. Moore. "Entanglement Entropy of Random Quantum Critical Points in One Dimension". In: *Physical Review Letters* 93 (26 I June 29, 2004). DOI: 10.1103/PhysRevLett.93.260602. arXiv: cond-mat/0406737. URL: http://arxiv.org/abs/cond-mat/0406737.

[4] Paola Ruggiero, Vincenzo Alba, and Pasquale Calabrese. "The Entanglement Negativity in Random Spin Chains". May 2, 2016. DOI: 10.1103/PhysRevB.94.035152. arXiv: 1605.00674. URL: http://arxiv.org/abs/1605.00674.

[5] Vincenzo Alba et al. "Unusual Area-Law Violation in Random Inhomogeneous Systems". In: *Journal of Statistical Mechanics: Theory and Experiment* 2019.2 (Feb. 26, 2019), p. 023105. ISSN: 1742-5468. DOI: 10.1088/1742-5468/ab02df. URL: https://iopscience.iop.org/article/10.1088/1742-5468/ab02df.

[6] G Vitagliano, A Riera, and J I Latorre. "Volume-Law Scaling for the Entanglement Entropy in Spin-1/2 Chains". In: *New Journal of Physics* 12.11 (Nov. 26, 2010), p. 113049. ISSN: 1367-2630. DOI: 10.1088/1367-2630/12/11/113049. URL: https://iopscience.iop.org/article/10.1088/1367-2630/12/11/113049.

[7] Daniel S. Fisher. "Random Antiferromagnetic Quantum Spin Chains". In: *Physical Review B* 50.6 (Aug. 1, 1994), pp. 3799–3821. ISSN: 0163-1829. DOI: 10.1103/PhysRevB.50.3799. URL: https://link.aps.org/doi/10.1103/PhysRevB.50.3799.

[8] Chandan Dasgupta and Shang-keng Ma. "Low-Temperature Properties of the Random Heisenberg Antiferromagnetic Chain". In: *Physical Review B* 22.3 (Aug. 1, 1980), pp. 1305–1319. ISSN: 0163-1829. DOI: 10.1103/PhysRevB.22.1305. URL: https://link.aps.org/doi/10.1103/PhysRevB.22.1305.

[9] Paola Ruggiero and Pasquale Calabrese. *Entanglement and Correlations in One-Dimensional Quantum Many-Body Systems*. Trieste: SCUOLA INTERNAZIONALE SUPERIORE DI STUDI AVANZATI, 2019.

[10] V. Vedral et al. "Quantifying Entanglement". In: *Physical Review Letters* 78.12 (Mar. 24, 1997), p. 2275. ISSN: 10797114. DOI: 10.1103/PhysRevLett.78.2275. arXiv: quant-ph/9702027. URL: https://journals.aps.org/prl/abstract/10.1103/PhysRevLett.78.2275 (visited on 08/21/2022).

[11] M. B. Plenio. "Logarithmic Negativity: A Full Entanglement Monotone That Is Not Convex". In: *Physical Review Letters* 95.9 (Aug. 26, 2005), p. 090503. ISSN: 0031-9007. DOI: 10.1103/PhysRevLett.95.090503. URL: https://link.aps.org/doi/10.1103/PhysRevLett.95.090503 (visited on 08/21/2022).

[12] Alfréd Rényi. "On Measures of Entropy and Information". In: *Berkeley Symposium on Mathematical Statistics and Probability* 4 (1961), pp. 547–561.

[13] Elliott H. Lieb and Mary Beth Ruskai. "Proof of the Strong Subadditivity of Quantum-mechanical Entropy". In: *Journal of Mathematical Physics* 14.12 (Nov. 3, 2003), p. 1938. ISSN: 0022-2488. DOI: 10.1063/1.1666274. URL: https://aip.scitation.org/doi/abs/10.1063/1.1666274 (visited on 08/22/2022).

[14] Don N. Page. "Average Entropy of a Subsystem". In: *Physical Review Letters* 71.9 (Aug. 30, 1993), pp. 1291–1294. ISSN: 0031-9007. DOI: 10.1103/PhysRevLett.71.1291. arXiv: gr-qc/9305007v2. URL: https://link.aps.org/doi/10.1103/PhysRevLett.71.1291 (visited on 08/20/2022).

[15] Michael M. Wolf. "Violation of the Entropic Area Law for Fermions". In: *Physical Review Letters* 96.1 (Jan. 13, 2006), p. 010404. ISSN: 10797114. DOI: 10.1103/PHYSREVLETT.96.010404/FIGURES/1/MEDIUM. arXiv: quant-ph/0503219. URL: https://journals.aps.org/prl/abstract/10.1103/PhysRevLett.96.010404 (visited on 08/24/2022).

[16] Pasquale Calabrese and John Cardy. "Entanglement Entropy and Quantum Field Theory". In: *Journal of Statistical Mechanics: Theory and Experiment* 2004.06 (June 12, 2004), P06002. ISSN: 1742-5468. DOI: 10.1088/1742-5468/2004/06/P06002. URL: https://iopscience.iop.org/article/10.1088/1742-5468/2004/06/P06002 (visited on 08/18/2022).

[17] Pasquale Calabrese, John Cardy, and Erik Tonni. "Entanglement Negativity in Quantum Field Theory". In: *Physical Review Letters* 109.13 (Sept. 28, 2012), p. 130502. ISSN: 0031-9007. DOI: 10.1103/PhysRevLett.109.130502. arXiv: 1206.3092. URL: https://link.aps.org/doi/10.1103/PhysRevLett.109.130502 (visited on 08/20/2022).

[18] Michael E. Fisher. "Renormalization Group Theory: Its Basis and Formulation in Statistical Physics". In: *Reviews of Modern Physics* 70.2 (Apr. 1, 1998), pp. 653–681. ISSN: 0034-6861. DOI: 10.1103/RevModPhys.70.653. URL: https://link.aps.org/doi/10.1103/RevModPhys.70.653.

[19] Ferenc Igloi and Cecile Monthus. "Strong Disorder RG Approach of Random Systems". Feb. 18, 2005. DOI: 10.1016/j.physrep.2005.02.006. arXiv: cond-mat/0502448. URL: http://arxiv.org/abs/cond-mat/0502448.

[20] Ferenc Iglói and Cécile Monthus. "Strong Disorder RG Approach – a Short Review of Recent Developments". In: *European Physical Journal B* 91.11 (2018). ISSN: 14346036. DOI: 10.1140/epjb/e2018-90434-8. arXiv: 1806.07684.

[21] Shang-keng Ma, Chandan Dasgupta, and Chin-kun Hu. "Random Antiferromagnetic Chain". In: *Physical Review Letters* 43.19 (Nov. 5, 1979), pp. 1434–1437. ISSN: 0031-9007. DOI: 10.1103/PhysRevLett.43.1434. URL: https://link.aps.org/doi/10.1103/PhysRevLett.43.1434.

[22] Jean-Philippe Bouchaud and Antoine Georges. "Anomalous Diffusion in Disordered Media: Statistical Mechanisms, Models and Physical Applications". In: *Physics Reports* 195.4-5 (Nov. 1990), pp. 127–293. ISSN: 03701573. DOI: 10.1016/0370-1573(90)90099-N. URL: https://linkinghub.elsevier.com/retrieve/pii/037015739090099N.

[23] Olexei Motrunich et al. "Infinite-Randomness Quantum Ising Critical Fixed Points". In: *Physical Review B - Condensed Matter and Materials Physics* 61.2 (June 21, 1999), pp. 1160–1172. DOI: 10.1103/PhysRevB.61.1160. arXiv: cond-mat/9906322v1. URL: http://arxiv.org/abs/cond-mat/9906322 (visited on 08/22/2022).

[24] C. Monthus. "On the Localization of Random Heteropolymers at the Interface between Two Selective Solvents". In: *The European Physical Journal B* 13.1 (Jan. 1, 2000), pp. 111–130. ISSN: 1434-6028. DOI: 10.1007/s100510050016. URL: http://link.springer.com/10.1007/s100510050016.

[25] Paola Ruggiero and Xhek Turkeshi. "Quantum Information Spreading in Random Spin Chains". June 6, 2022. DOI: 10.48550/arXiv.2206.02934. arXiv: 2206.02934. URL: http://arxiv.org/abs/2206.02934 (visited on 08/21/2022).

[26] Nicolas Laflorencie. "Scaling of Entanglement Entropy in the Random Singlet Phase". Apr. 18, 2005. DOI: 10.1103/PhysRevB.72.140408. arXiv: cond-mat/0504446. URL: http://arxiv.org/abs/cond-mat/0504446.

[27] Maurizio Fagotti, Pasquale Calabrese, and Joel E. Moore. "Entanglement Spectrum of Random-Singlet Quantum Critical Points". In: *Physical Review B - Condensed Matter and Materials Physics* 83.4 (Jan. 31, 2011), p. 045110. ISSN: 10980121. DOI: 10.1103/PHYSREVB.83.045110/FIGURES/10/MEDIUM. arXiv: 1009.1614. URL: https://journals.aps.org/prb/abstract/10.1103/PhysRevB.83.045110 (visited on 08/25/2022).

[28] J D Cresser. *Quantum Physics Notes*. 2011.

[29] Wolfgang Pauli. “Exclusion Principle and Quantum Mechanics”. In: (1946).

[30] Tom Lancaster and Stephen J Blundell. *Quantum Field Theory for the Gifted Amateur*. 5. Oxford: Oxford University Press, 2014. ISBN: 978-0-19-969933-9.

[31] Glen Bigan Mbeng, Angelo Russomanno, and Giuseppe E. Santoro. “The Quantum Ising Chain for Beginners”. Version 1. In: (2020). DOI: 10.48550/ARXIV.2009.09208. URL: https://arxiv.org/abs/2009.09208 (visited on 08/28/2022).

[32] Ingo Peschel and Viktor Eisler. “Reduced Density Matrices and Entanglement Entropy in Free Lattice Models”. In: *Journal of Physics A: Mathematical and Theoretical* 42.50 (Dec. 2009), p. 504003. ISSN: 1751-8121. DOI: 10.1088/1751-8113/42/50/504003. URL: https://doi.org/10.1088/1751-8113/42/50/504003 (visited on 08/30/2022).